Bioconjugate Chemistry

Article

Functionally Versatile and Highly Stable Chelator for 111In and 177Lu: Proof-of-principle Prostate Specific Membrane Antigen Targeting

LILY LI, María de Guadalupe Jaraquemada-Peláez, Hsiou-Ting Kuo, Helen Merkens, Neha Choudhary, Katrin Gitschalter, Una Jermilova, Nadine Colpo, Carlos Uribe-Munoz, Valery Radchenko, Paul Schaffer, Kuo-Shyan Lin, Francois Benard, and Chris Orvig

Bioconjugate Chem., **Just Accepted Manuscript** • DOI: 10.1021/acs.bioconjchem.9b00225 • Publication Date (Web): 22 Apr 2019

ACS Publications

is published by the American Chemical Society. 1155 Sixteenth Street N.W., Washington, DC 20036

Functionally Versatile and Highly Stable Chelator for ^{111}In and ^{177}Lu: Proof-of-principle Prostate Specific Membrane Antigen Targeting

Lily Li[a,c], María de Guadalupe Jaraquemada-Peláez[a], Hsiou-Ting Kuo[d], Helen Merkens[d], Neha Choudhary[a,c], Katrin Gitschtaler[d], Una Jermilova[a], Nadine Colpo[d], Carlos Uribe-Munoz[d], Valery Radchenko[b,c], Paul Schaffer[c], Kuo-Shyan Lin[d], François Bénard[d*], Chris Orvig[a*]

[a] Medicinal Inorganic Chemistry Group, Department of Chemistry, University of British Columbia, 2036 Main Mall, Vancouver, British Columbia V6T 1Z1, Canada

[b] Department of Chemistry, University of British Columbia, 2036 Main Mall, Vancouver, British Columbia V6T 1Z1, Canada

[c] Life Sciences Division, TRIUMF, 4004 Wesbrook Mall, Vancouver, British Columbia V6T 2A3, Canada

[d] Department of Molecular Oncology, BC Cancer, 675 West 10th Ave, Vancouver, British Columbia V5Z 1L3, Canada

Abstract

Here, we present the synthesis and characterization of a new potentially nonadentate chelator, H_4pypa and its bifunctional analog $^tBu_4$pypa-C7-NHS conjugated to PSMA (prostate-specific membrane antigen) - targeting peptidomimetic (Glu-urea-Lys). H_4pypa is very functionally versatile and biologically stable. Compared to the conventional chelators (e.g. DOTA, DTPA), H_4pypa has outstanding affinities for both ^{111}In (EC, $t_{1/2}$ ~2.8 d) and ^{177}Lu (β^-,γ, $t_{1/2}$~6.64 d). Its radiolabeled complexes were achieved at >98% radiochemical yield, RT within 10 minutes, at ligand concentration as low as 10^{-6} M, with excellent stability in human serum over at least 5-7 days (<1% transchelation). The thermodynamic stabilities of the $[M(pypa)]^-$ complexes (M^{3+} = In^{3+}, Lu^{3+}, La^{3+}) were dependent on the ionic radii, where the smaller In^{3+} has the highest pM value (30.5), followed by Lu^{3+} (22.6) and La^{3+} (19.9). All pM values are remarkably higher than those with DOTA, DTPA, H_4octapa, H_4octox and H_4neunpa. Moreover, the facile and versatile bifunctionalization enabled by the *p*-OH group in the central pyridyl bridge of the pypa scaffold (compound **14)** allows incorporation of a variety of linkers for bioconjugation through easy nucleophilic substitution. In this work, an alkyl linker was selected to couple H_4pypa to a PSMA-targeting pharmacophore, proving that the bioconjugation sacrifices neither the tumor-targeting

nor the chelation properties. The biodistribution profiles of ^{111}In- and ^{177}Lu-labeled tracers are different, but promising, with the ^{177}Lu analog particularly outstanding.

Introduction

The potential of radionuclides in cancer diagnosis and therapy has been recognized for decades since the discovery of radioactivity in 1901.[1] The specificity and minimal invasiveness of targeted radionuclide therapy compared to chemotherapy has poised the field for further growth, stimulated by the technological advancements in production of both radionuclides and biological targeting vectors (e.g. peptides and monoclonal antibodies). The biological safety of the radiometal is ensured by a stably bound chelator coupled to a bio-targeting vector via a covalent linkage, which also modulates the pharmacokinetics of the whole. [2-4]

An ideal chelator should possess rapid complexation kinetics and strong affinity for the radiometal ion at mild conditions (RT, <15 minutes complexation), as well as high versatility of linker incorporation (i.e. bifunctionalization) without sacrificing the coordination integrity. Although a small peptidomimetic conjugate usually has higher tolerance to the harsh radiolabeling conditions (e.g. 60-90 ^{o}C for 1,4,7,10-tetraazacyclododecane-1,4,7,10-tetraacetic acid, DOTA, Chart 1), fast and quantitative radiolabeling at room temperature facilitate handling and avoid potential degradation of the product. One of the benefits is that instead of relying on central manufacturing, clinicians can conveniently prepare the radioactive tracer in a local hospital, which mimics the existing practice for ^{99m}Tc kits.[5] In terms of bifunctionalization, most of the commercial chelators including DOTA and diethylenetriamine-pentaacetic acid (DTPA), lack a convenient spot for adding a linker. The cumbersome functionalization on the polyamine backbone or the sacrifice of a pendant arm can complicate the synthesis while restricting the linker variety, or even reduce the complex stability.[6-8] Additionally, a practically and clinically useful chelator should accommodate (a pair of) theranostic isotopes (e.g. ^{177}Lu, ^{111}In, $^{86/90}$Y, $^{44/47}$Sc) for an accurate study of dosimetry to achieve optimal therapeutic effects. In this regard, ^{177}Lu ($t_{1/2}$ ~ 6.64 days) is well-recognized for treating small and metastatic tumors with its low-energy β^- particles (maximum 498 keV),[9] along with two useful γ emissions (208 keV and 113 keV) for SPECT imaging, rendering it an excellent theranostic isotope with a favorable half-life.[10] The high thermal neutron capture cross section of ^{176}Lu also allows direct production of ^{177}Lu [^{176}Lu(n,γ)^{177}Lu] with high specific activity at multi-Curie activity levels to meet the impending demand for targeted cancer therapy.[11, 12] Of course,

no-carrier-added (n.c.a.) ^{177}Lu can also be produced through an indirect route (^{176}Yb(n,γ)^{177}Yb→ ^{177}Lu).[12, 13] Another potential theranostic radioisotope is the γ-ray and Auger-electron-emitting ^{111}In ($t_{1/2}$ ~ 2.8 days), which has proved induction of cytocidal double-strand break (DSBs) upon internalization and translocation to the nucleus of the tumor cells, besides its widespread applications in SPECT imaging. [2, 14-17]

To overcome the practical concerns on the radiolabeling conditions and the complex stability encountered with the current commercial chelators, we report herein the synthesis and characterization of a new potentially nonadentate pyridinecarboxylate-based ligand, H_4pypa and a bifunctional H_4pypa conjugated to glutamate-urea-lysine-based PSMA (prostate-specific membrane antigen)-targeting pharmacophore for prostate cancer (PCa) targeting. PCa is the most common cancer in men in the United States accounting for around 26,730 deaths in 2017.[18] PSMA is primarily expressed in normal human prostate epithelium, but is up-regulated in prostate cancer cells, even more in de-differentiated, metastatic and hormone-refractory carcinomas, rendering it an attractive target in PCa.[19] The current FDA-approved ^{111}In-capromab pendetide scan (ProstaScint® scan) has several drawbacks such as inducing the formation of human anti-mouse antibody (HAMA) and targeting the intracellular epitope of PSMA, which somewhat limit its applications.[20, 21] The Glu-urea-Lys PSMA inhibitor adopted in this study was developed by Maresca et al.,[22] and the lipophilic spacer was suggested to improve the pharmacokinetics by Benešová et al. who conjugated the whole moiety to DOTA (a.k.a. PSMA617) for ^{68}Ga and ^{177}Lu radiolabels.[23] In this paper, we show that both H_4pypa and its PSMA-targeting counterpart radiolabel ^{111}In and ^{177}Lu in excellent yield and stability with the LNCaP-tumor targeting ability preserved. Moreover, the thermodynamic stabilities of M-pypa systems (M=In^{3+}, Lu^{3+}, La^{3+}) measured as pM are considerably higher than those with DOTA, DTPA, H_4octapa, H_4octox and H_4neunpa. In addition to chelation, a significant advantage of the pyridyl bridge is the facile and versatile linker attachment via the central hydroxyl group. Undeniably, linkages play a pivotal role in the biological behavior of the radiochelate, particularly the small peptide conjugates.[23-27] Therefore, this versatility provides flexibility in not only the chemical properties of the whole (e.g. hydrophilic, hydrophobic), but also the targeting vectors associated (e.g. peptide, antibody, antibody fragment, nanoparticles).[3] The combination renders H_4pypa a promising theranostic chelating agent for many different cancer treatments, despite the focus here on prostate cancer.

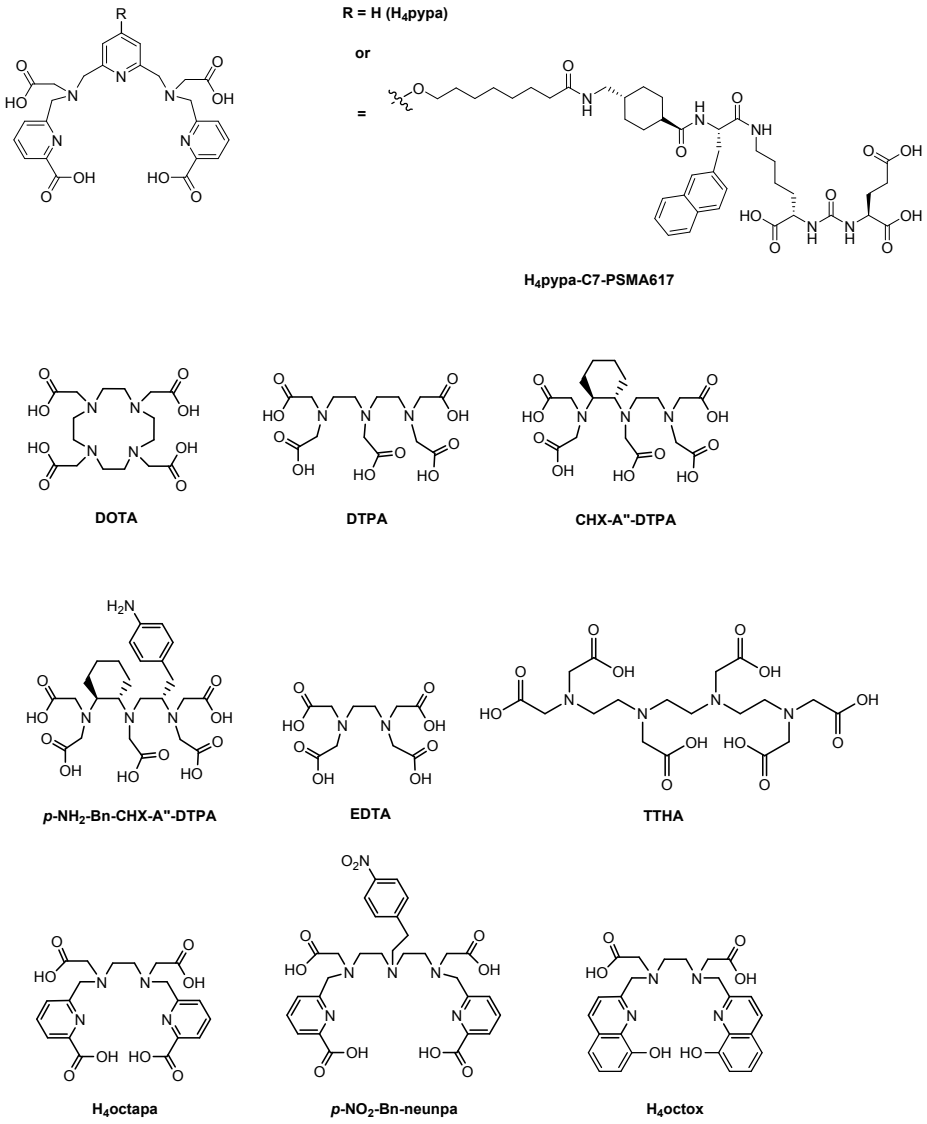

Chart 1. Chemical structures of selected chelators.

Result and Discussion

Synthesis and Characterization

Our group has established a significant library of non-macrocyclic chelators, including picolinate and hydroxyquinoline derivatives, to target different radionuclides.[28-30] H_4pypa is a new member of the picolinate-arm-based ligand family, designed to accommodate medium-to-large radioisotopes (e.g. ^{177}Lu, ^{111}In, ^{44}Sc, $^{86/89}$Y) in its potentially nine-coordinating cavity, securing the metal ion with the rigid pyridyl cap on which a variety of linkers can be attached efficiently for bioconjugation. As depicted in Scheme 1, the arm and pyridyl backbone of the non-bifunctional

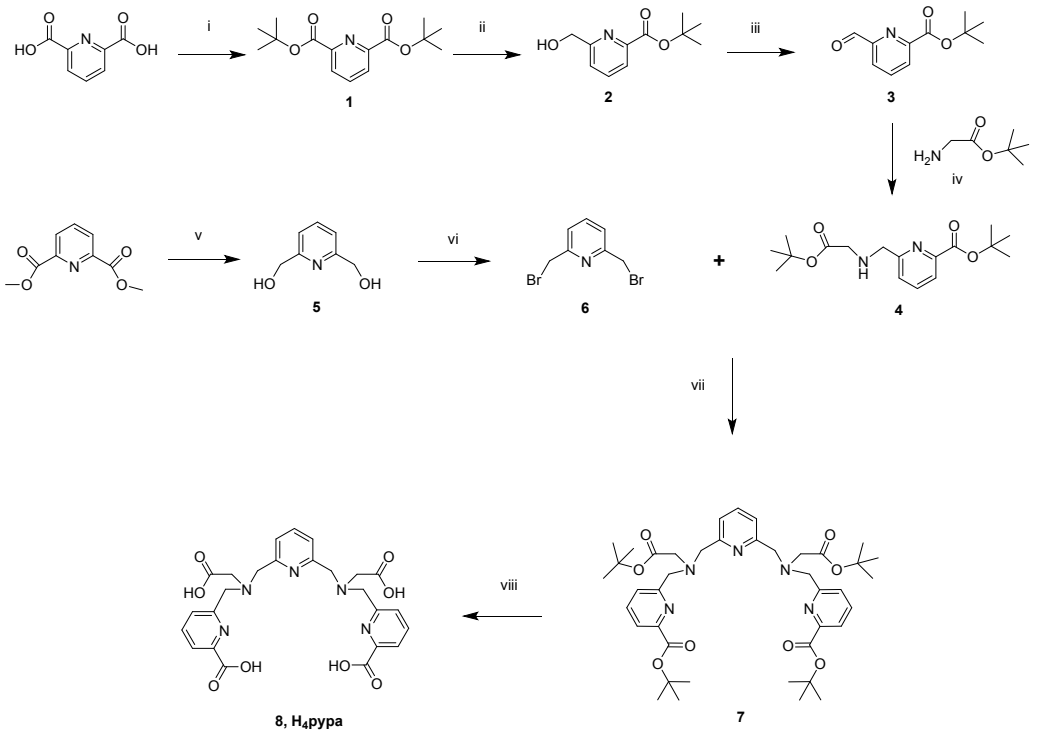

Scheme 1. Reagents and conditions: i) DCC, tert-butyl alcohol, DCM, RT, overnight, 50%; ii) $NaBH_4$, dry MeOH, RT, 3-4 h, 72%; iii) SeO_2, 1,4-dioxane, 100°C, overnight, 56%; iv) 1. Dry MeOH, RT, 1 h; 2. $NaBH_3CN$, dry MeOH, 3 h, 70%; v) $NaBH_4$, dry MeOH, RT, 12 h, 92%; vi) PBr_3, dry $CHCl_3$/ACN, 60 °C, 18 h, 70%; vii) K_2CO_3, dry ACN, 60 °C, 24 h, 70%; viii) TFA/DCM, RT, overnight, 70%

H_4pypa were strategically synthesized individually and then assembled in one convergence step for higher synthetic efficiency. The backbone was synthesized by first reducing the starting material dimethyl 2,6-pyridinedicarboxylate to pyridine-2,6-diyl-dimethanol (**5,** 92%), followed by bromination with phosphorus tribromide, to give the dibromo-derivative **(6**, 70%) which was coupled with 2 equivalents of the picolinate-acetate arm moiety (**4**). The tert-butyl esters on arm **4** were selected for the compatibility with solid-phase peptide coupling and it was synthesized through one-pot Schiff base formation and reduction using the aldehyde (**3**) and tert-butyl glycinate (70%). Compound **3** was prepared by converting 2,6-pyridinedicarboxylic acid to the corresponding tert-butyl-ester analogue (**1**), followed by monoreduction with sodium borohydride ($NaBH_4$) to give compound **2** and subsequent oxidation to aldehyde (**3**) by selenium(IV) oxide (SeO_2) (cumulative yield ~20%). Finally, both pendant arm (**4**) and pyridyl bridge (**6**) were connected through S_N2 nucleophilic substitution (**7**, 70%) and then deprotection was followed to give H_4pypa (**8**, 70%). Purification with high-performance liquid chromatography (HPLC) yielded the final product as a trifluoroacetic acid (TFA) salt (H_2pypa·2TFA·1.7H_2O as determined by

elemental analysis). Regarding the bifunctional H_4pypa (Scheme 2), commercially available chelidamic acid monohydrate was selected as the backbone starting material. After converting the carboxylic acids to methyl esters (**9, >**99%**)**, the *p*-OH group on the pyridyl moiety was protected with benzyl bromide (**10**, 64%).

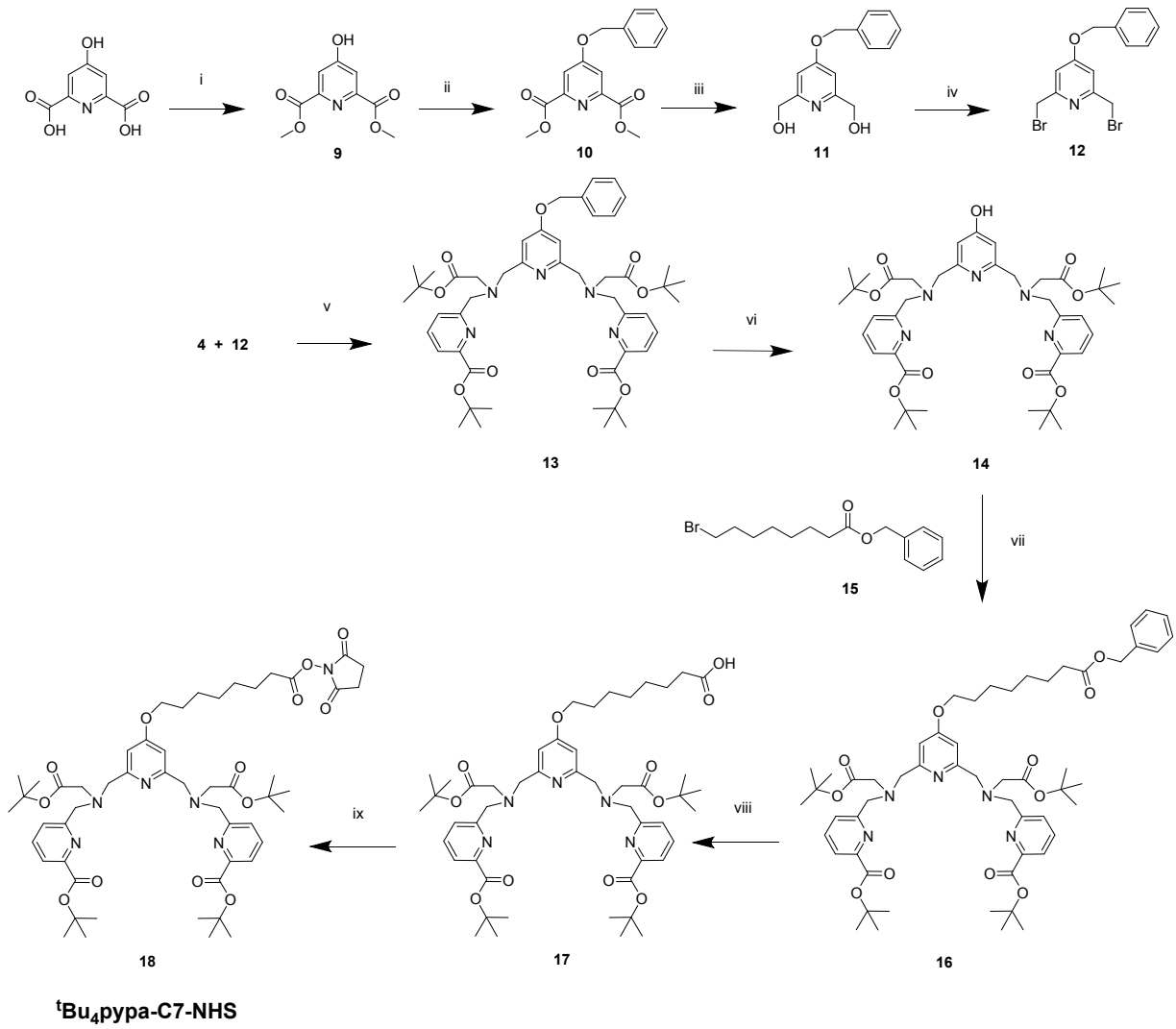

Scheme 2. Reagents and conditions. i) $SOCl_2$, MeOH, RT-60 °C, 26 h, >99%; ii) BnBr, ACN, K_2CO_3, 60 °C, overnight, 64%; iii) $NaBH_4$, dry MeOH, RT, overnight, 82%; iv) PBr_3, dry $CHCl_3$/dry ACN, 60 °C, overnight, 70%; v) K_2CO_3, dry ACN, 30 °C, 24 h, 73%; vi) Pd/C (10% w/w), H_2 (g), MeOH, RT, overnight; vii) K_2CO_3, dry THF, RT-35 °C, 24 h, 90%; viii) Pd/C, MeOH, RT, overnight, 88%; ix) NHS, EDCI, dry ACN, RT, overnight, 86%.

Similar to the H_4pypa preparation, the methyl esters in compound **10** were reduced to alcohols (**11**, 82%), and then brominated to give compound **12** (70%), which was coupled to arm **4** through the aforementioned protocol to yield the protected pypa (**13**, 73%). Following debenzylation with Pd/C-catalyzed hydrogenation, the alkyl linker was added through S_N2 nucleophilic substitution

to give compound **16** (90%). Deprotection and activation with 1-ethyl-3-(3-dimethylaminopropyl)carbodiimide hydrochloride/ N-hydroxysuccinimide (EDCI/NHS) generated the activated ester (**18**, 76% over 2 steps), which was coupled to the PSMA-targeting-peptide-bound resin by using N,N-diisopropylethylamine (DIPEA) in dry DMF overnight. After the coupling finished, the peptide-bioconjugate was deprotected and simultaneously cleaved from the resin with 95/5 trifluoroacetic acid (TFA)/triisopropylsilane (TIS) for 2 hours at room temperature to give H_4pypa-C7-PSMA617 (Chart 1).

Metal Complexation and Characterization

The complexation with non-radioactive In^{3+}, Lu^{3+} and La^{3+} ions was studied and the complexes were characterized with NMR spectroscopy (^{1}H, ^{13}C and HSQC) and high-resolution electrospray ionization mass spectrometry (HR-ESI-MS). Being the largest lanthanide, La^{3+} is also of interest in its complexation with H_4pypa in comparison with that of Lu^{3+} which is the smallest in the series.[31] All three complexes appeared to be rigid coordination complexes with no observable fluxionality, as confirmed by the sharply resolved ^{1}H NMR peaks and the absence of extra hydrogen and carbon signals in ^{1}H and ^{13}C NMR spectra (Figures S15-S22). In the case of $[In(pypa)]^-$, all the carbons in the complex were chemically distinct from one another, while there were three pairs of visible diastereotopic methylene protons (2.94 and 3.22 ppm, ^2J =17.6 Hz; 3.78 and 3.91 ppm, ^2J =17.1 Hz; 4.10 and 4.44, ^2J=17.4) (Figures 1A and S19), and each doublet accounted for only one hydrogen atom; the rest were overlapping with the water signal (revealed by the interaction with the adjacent carbon atom shown in ^{1}H-^{13}C HSQC, Figure S20B), indicating the asymmetry in the complex in solution state. The asymmetry was also observed in $[La(pypa)]^-$ which appeared in solution as a single isomer (Figures 1A and S21). On the other hand, $[Lu(pypa)]^-$ presented in solution as a symmetric complex, marked by the unchanged number of carbon signals (Figure S16), as well as the consistent ^{1}H aromatic pattern (two triplets - 8.21 and 7.85 ppm, and three doublets - 8.05, 7.80 and 7.44 ppm) compared with the uncomplexed chelator (Figures 1A and S15). Furthermore, the complex only exhibited two pairs of diastereotopic protons (3.49 and 3.98 ppm, ^2J=17.0 Hz; 4.07 and 4.39 ppm, ^2J=14.7 Hz), while the last pair of methylene-H appeared as a sharp singlet at pH = 1.5 but a clear doublet at pH = 11.5 (Figure 1B). However, the much smaller splitting of the peak compared to the other diastereotopic pairs implied a much weaker, or perhaps farther interaction with the Lu^{3+} ion. Additionally, this pair of methylene

protons belonged to a carbon that has a very similar chemical shift with another methylene carbon which suggested that both of them might be adjacent to the pyridyl group instead of the carboxylic acid on the acetate arms (Figure S17). Interestingly, as determined by potentiometric titration, the [Lu(Hpypa)] species deprotonates at pH = 3.35-3.60 which can be reasonably assigned to the protonated central pyridine. In this case, it could be inferred that the interaction between the pyridyl bridge and the Lu^{3+} ion is weaker when the central pyridine-N atom is protonated at low pH, and is increased when is deprotonated at higher pH, which however, was not as strong as that with the acetate and picolinate arms. This phenomenon could also be explained by the relatively small atomic size and the hard nature of Lu^{3+}.[31]

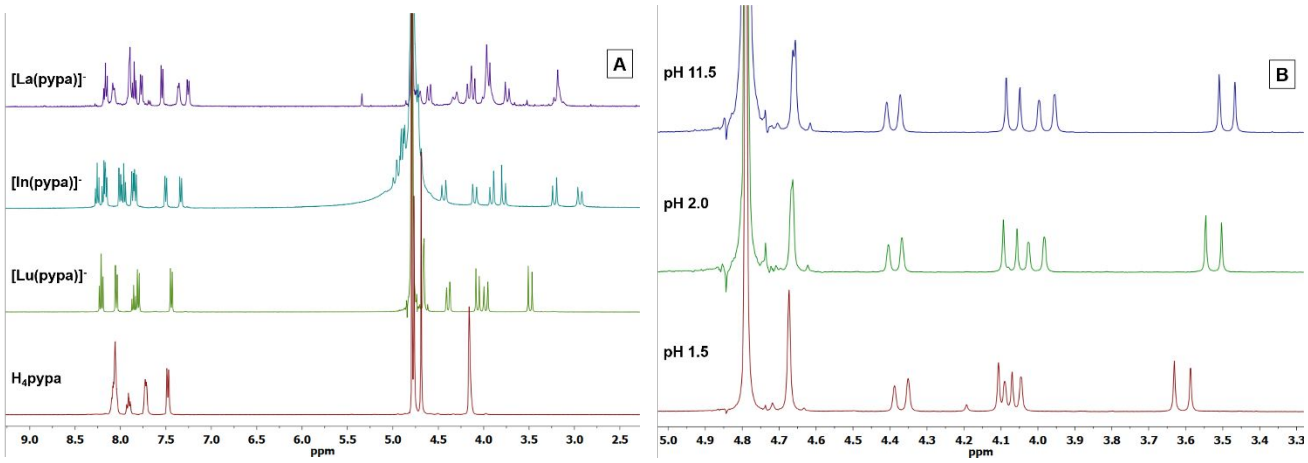

Figure 1. (A) Partial ^{1}H NMR spectra of $[La(pypa)]^-$, $[In(pypa)]^-$, $[Lu(pypa)]^-$, H_4pypa (top-bottom) (D_2O, 400 MHz, 298 K). **(B)** Partial ^{1}H NMR spectra of $[Lu(pypa)]^-$ at pH=11.5, 2.1 and 1.5 (top-bottom) (D_2O, 400 MHz, 298 K).

X-ray Crystallography

X-ray quality single crystals of H[Lu(pypa)] were obtained by the slow evaporation of 1:1 $LuCl_3$ and H_4pypa solutions in water after adjustment of pH to 2. The ORTEP diagram of $[Lu(pypa)]^-$ is shown in Figure 2 and its crystallographic data can be found in the Supporting Information. From Figure 2, it can be seen that at pH 2 two of the carboxylic groups of the ligand are protonated. The H atom attached to O2 (picolinic -COOH) is half occupied in one of the asymmetric units, as is the case with Cl atom which is equally shared by two asymmetric units. While the H atom attached to O6 (backbone -COOH) is fully occupied, hence the overall charge is neutral. The Lu(III) ion is nine-coordinated by the N_5O_4 donor atoms of the ligand. Selected bond distances and bond angles are provided in Table 1. The geometry is distorted but nevertheless, the structure provides the vital visual insight to the coordination environment of the Lu(III) ion. It can be clearly seen from the structure that Lu(III) sits in the cavity of the H_4pypa ligand, capped by the pyridyl group. Also, the

preference of Lu(III) for O-donor atoms can be seen from the shorter Lu-O bond distances compared to longer Lu-N bonds.

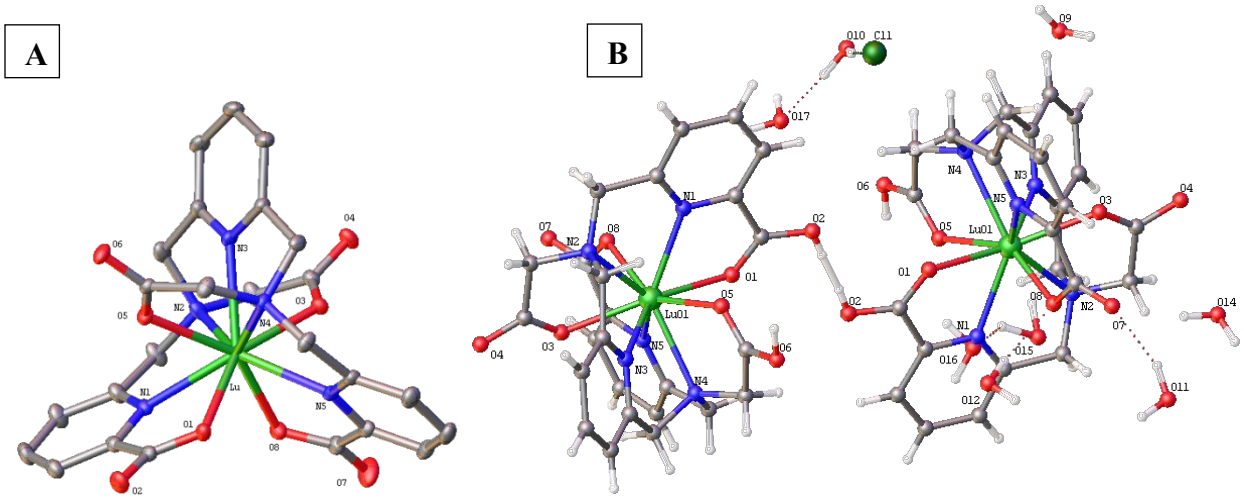

Figure 2. ORTEP diagrams of the anion in (A) H[Lu(pypa)] (B) $C_{50}H_{79}ClLu_2N_{10}O_{33}$

Table 1. Selected bond lengths and bond angles in $[Lu(pypa)]^-$.

Bond length/Å			Bond Angle/°			
Atom	**Atom**	**Length/Å**	**Atom**	**Atom**	**Atom**	**Angle/°**
Lu	O1	2.3266(17)	O3	Lu	N2	70.14(6)
Lu	O3	2.3333(17)	O5	Lu	N5	129.28(6)
Lu	O5	2.3559(17)	O8	Lu	N5	68.64(7)
Lu	O8	2.2954(17)	N1	Lu	N2	67.31(6)
Lu	N1	2.4181(19)	N3	Lu	N2	67.44(7)
Lu	N2	2.537(2)	N3	Lu	N4	66.17(6)
Lu	N3	2.451(2)				
Lu	N4	2.553(2)				
Lu	N5	2.3845(19)				

Solution Thermodynamics

When evaluating ligands for metal complexation, knowledge of the basicity of the different ionizable and non-ionizable protons is essential because the metal ion will compete for replacing them at the basic sites. H_4pypa possesses nine protonation sites, and in this work, we determined the acidity constants for all of them. Combined potentiometric-spectrophotometric titrations were

carried out by following spectral changes in the absorption band of the picolinate chromophore for the first seven protonation equilibria and UV in batch spectrophotometric titrations for the last two equilibria, as they deprotonate at a pH below the electrode threshold. The different absorption features related to the above-mentioned equilibria as the pH is raised are presented in Figure S51. Table 2 presents the protonation constants calculated from the experimental data using the HypSpec2014[32] and Hyperquad2013[33] programs. Figure S52A presents one of the titration curves of an acidified solution of H_4pypa·2TFA·1.7H_2O and it shows that nine equivalents of base (NaOH) were consumed in the titration. The speciation plots of different species of H_4pypa in Figure S52b were calculated from the protonation constants in Table 2 with the Hyss software.[34]

Table 2. Protonation constants of H_4pypa at 25.0 °C, I = 0.16 M NaCl.

Equilibrium Reaction	log β	log K
$L^{4-} + H^+ \leftrightarrows HL^{3-}$	7.78 (1)	7.78 (1)
$HL^{3-} + H^+ \leftrightarrows H_2L^{2-}$	14.56 (1)	6.78 (1)
$H_2L^{2-} + H^+ \leftrightarrows H_3L^-$	18.25 (1)	3.69 (1)
$H_3L^- + H^+ \leftrightarrows H_4L$	21.27 (1)	3.02 (1)
$H_4L + H^+ \leftrightarrows H_5L^+$	23.50 (2)	2.23 (2)
$H_5L^+ + H^+ \leftrightarrows H_6L^{2+}$	25.56 (6)	2.06 (6)
$H_6L^{2+} + H^+ \leftrightarrows H_7L^{3+}$	27.26 (2)	1.70 (2)
$H_7L^{3+} + H^+ \leftrightarrows H_8L^{4+}$	26.89 (1) [(a)]	-0.37 (1) [(a)]
$H_8L^{4+} + H^+ \leftrightarrows H_9L^{5+}$	26.31 (2) [(a)]	-0.58 (2) [(a)]

(a) from in batch UV spectrophotometric titrations, not evaluated at constant ionic strength (0.16 M NaCl).

The structure of H_4pypa resembles that of H_4octapa,[28, 35] with the difference in the backbone: in H_4pypa, a pyridyl ring bridges the two tertiary nitrogen atoms. Not surprisingly, also in this case, the two most acidic protons (species H_9L^{5+} and H_8L^{4+}, pK_1 = -0.58 (2) and pK_2 = -0.37 (1)) can be attributed to the deprotonation of the pyridine nitrogen atoms in the picolinate moieties based on the bigger spectral changes in the band of this chromophore. Following that, the species H_7L^{3+} and H_6L^{2+} deprotonate with pK_3 = 1.70 (2) and pK_4 = 2.06 (6), respectively, and they can be attributed to the deprotonation of the two acetate carboxylic acids. Species H_5L^+ and H_4L deprotonate with pK_5 = 2.23 (2) and pK_6 = 3.02 (1), respectively, and are attributed to the picolinate-COOH. The last three dissociation steps are assigned to the tertiary nitrogen atoms and the central pyridine

nitrogen (species H_3L^-, H_2L^{2-} and HL^{3-}). Comparing the pK_a values for the tertiary nitrogen atoms of H_4pypa (pK_8 = 6.78 (1) and pK_9 = 7.78 (1)) to those of H_4octapa (pK_7 = 5.43 (2) and pK_8 = 8.58 (1))[35], the ΔpK_a for those equilibria is of 1 unit in H_4pypa while it is 3.1 units in H_4octapa. This can be explained for the larger charge repulsion in H_4octapa compared to H_4pypa when the two nitrogen atoms are protonated. The pK_7 = 3.69 (1) can be allocated therefore to the central pyridine nitrogen atom.

Complex Formation Equilibria of H_4pypa with In(III), Lu(III) and La(III)

Complex formation equilibria studies of H_4pypa with metal ions of relevant interest in radiopharmaceutical chemistry were carried out by different methods. The extent to which the metal complexation occurred even at pH ~2 was too high to allow a direct determination of the stability constants for the $[ML]^-$ species by simple potentiometric titrations of H_4pypa with the respective metal ions. Protonated species of the metal complexes, MHL, were found with H_4pypa and In^{3+}, Lu^{3+} and La^{3+} ions by competition methods; ligand-ligand competition methods with the competing ligand TTHA were used for In^{3+} and Lu^{3+} ions, while for La^{3+}, EDTA was used as a competitor. Additionally, acidic in batch UV spectrophotometric titrations were carried out for all M^{3+}-H_4pypa systems (M^{3+} = In^{3+}, Lu^{3+} and La^{3+}) (Figures S53-S55). Once the stability constants for the MHL species (log K_{MHL}) were known, the direct potentiometric method was used to determine the stability constants of the $[ML]^-$ and $[M(OH)L]^{2-}$ species for In^{3+} and Lu^{3+}, and $[ML]^-$ and $[M_2L_2(OH)]^{3-}$ species for La^{3+}. Potentiometric and spectrophotometric experimental data were refined using the HypSpec2014[32] and Hyperquad2013[33] programs and the stability constants are presented in Table 3.

The metal complex stability of the $[ML]^-$ species formed (log K_{ML}) with H_4pypa follows the order $In^{3+} > Lu^{3+} > La^{3+}$. The size and the acid character of the metal ion definitely play a role on its metal complex stability, and from these results, the cavity of H_4pypa seems best fitted for the smaller In^{3+}.

In order to compare the excellent stability of M^{3+}-H_4pypa complexes with the stability of other metal complexes involving different chelators, it is necessary to use a parameter that takes into account not just the stability of the metal complexes, but also the basicity and the denticity of the different chelators to be compared. The parameter pM is widely used in medicinal inorganic

chemistry for this purpose, and is a measurement of the metal sequestering ability of a determined chelator towards an specific metal ion; it is defined as $-\log [M^{n+}]_{free}$ at [ligand] = 10 μM and $[M^{n+}]$ = 1 μM at pH = 7.4.[36] In Figure 3A, the pM values for the most relevant chelators currently used in the radiopharmaceutical field have been plotted for the metals of our interest and the H_4pypa performance exceeds that of all the other chelators. Additionally, Figure 3B shows the importance of the basicity of different chelators on the metal sequestration ability or pM values; in particular, it shows the metal sequestering ability in terms of pLu^{3+} as the pH is raised. For ligands with lower overall basicities (Table S3), the protons will compete less with the metal ion and will show complexation from lower pHs and in a broader pH range. This effect is more dramatic when comparing the metal affinity of H_4pypa and H_4octox towards Lu^{3+}. Although the overall stability constant of $[Lu(octox)]^-$ ($\log K = 24.66(1)$)[37] is higher than that of $[Lu(pypa)]^-$ ($\log K = 22.02(6)$), the higher basicity of H_4octox prevents Lu^{3+} scavenging at lower pHs and more importantly, at physiological pH = 7.4, the effectiveness of H_4octox is 4.4 units lower than that of H_4pypa. These promising solution thermodynamics findings reveal H_4pypa as an excellent chelator for further studies *in vitro* and *in vivo*, particularly for the theranostic ^{177}Lu isotope.

Table 3. Stepwise stability constants ($\log K$) of H_4pypa complexes with In^{3+}, Lu^{3+} and La^{3+}.

Equilibrium reaction	In^{3+}	Lu^{3+}	La^{3+}
$M^{3+} + L \leftrightarrows ML$	29.99(4)[a]; 30.13(3)[b]	22.02(6)[a]; 22.20(2)[b]	19.74(3)[d]; 19.54(2)[b]
$ML + H^+ \leftrightarrows MHL$	4.06(5)[a]; 3.80(1)[c]	3.35(8)[a]; 3.60(6)[c]	2.99(4)[d]; 3.24(5)[c]
$M(OH)L + H^+ \leftrightarrows ML$	10.59(7)[a]; 10.44(4)[b]	10.77(8)[a]; 10.86(3)[b]	-
$M_2L_2(OH) + H^+ \leftrightarrows M_2L_2$	-	-	33.88(7)[d]; 34.40(6)[b]
pM[e]	**30.5**	**22.6**	**19.9**

a) ligand-ligand potentiometric competition with H_6ttha at I = 0.16 M (NaCl) and 25 °C; b) potentiometric titrations at I = 0.16 M (NaCl) and 25 °C; c) in-batch acidic spectrophotometric competition at 25 °C, not evaluated at constant I = 0.16 M (NaCl); d) ligand-ligand potentiometric competition with H_4edta at I = 0.16 M (NaCl) and 25 °C; e) pM is defined as $-\log [M]_{free}$ at [L] = 10 μM, [M] = 1 μM and pH = 7.4. Charges are omitted for clarity.

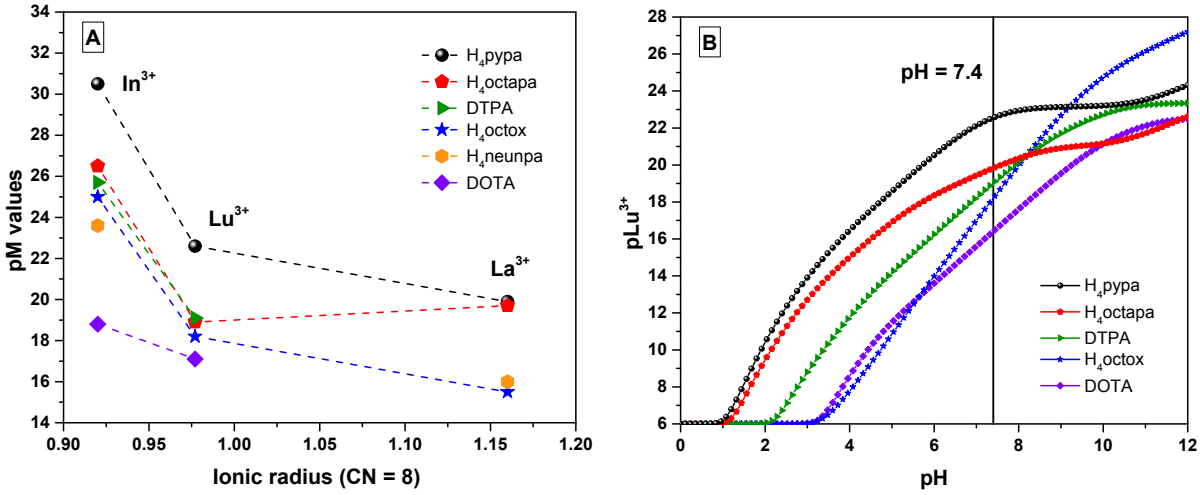

Figure 3. (A) pM values *vs* ionic radius[31] for M^{3+}- ligand complexes (CN = 8); **(B)** Lu^{3+} scavenging ability of different ligands as the pH is raised from 0-12, $[Lu^{3+}] = 1 \times 10^{-6}$ M and [ligand] = 1×10^{-5} M. Solid line in B at indicates physiological pH (7.4). Stability constants and acidity constants of ligands other than H_4pypa used for the plotting are reported in Tables S3-S4.

Radiolabeling and Human Serum Challenge Experiments

In most receptor targeting radiotracer formulations, the unlabeled receptor targeting vector is preferably kept minimum to ensure that the receptor is not saturated by unlabeled targeting motif, which in other words is to maximize the apparent molar activity.[38] Quantitative radiolabeling at mild conditions (RT, 10 minutes) with low ligand concentration and low ligand/radiometal (mol/mol) (L/M) ratio obviates the need of post-labeling HPLC purification to attain high apparent molar activity, which has significant impact on the biological profile. Fendler et al. reported that high apparent molar activity of ^{177}Lu-PSMA-617 was associated with higher tumor uptake, more prominent DNA damage and more effective tumor growth inhibition.[39] In our study, concentration-dependent radiolabeling was applied to determine the lowest ligand (H_4pypa and H_4pypa-C7-PSMA617) concentration required for quantitative radiometalation with both ^{177}Lu and ^{111}In, while the corresponding L/M ratio was adjusted afterwards using a mixture of no-carrier-added (n.c.a.) radioactive and non-radioactive isotopes from diluted AAS standards (i.e. $^{177/nat}$Lu or $^{111/nat}$In). All radiolabeling studies were performed in triplicate. Firstly, both H_4pypa and H_4pypa-C7-PSMA617 radiolabeled ^{177}Lu and ^{111}In quantitatively (>98% radiochemical yield, RCY) in 10 minutes with 10^{-6} M ligand concentration at RT and pH=7 (Figure 4A), indicated by a single sharp signal at the baseline of the iTLC-SA plate developed with EDTA solution (50 mM,

pH = 5.5), which is consistent with the well-separated radiopeaks of the free metal and the complex on the HPLC radiotraces (t_R = 12.9 and 10.4 minutes for ^{177}Lu- and ^{111}In-pypa complexes; 15.0 and 14.1 minutes for ^{177}Lu- and ^{111}In-pypa-C7-PSMA617 complexes) (Figures S45-S50). The corresponding complexes were highly kinetically inert with <1% transmetalation to the serum proteins over at least 7 days for both ^{177}Lu complexes and 5 days for [^{111}In][In(pypa)]$^-$ (Figure 4B), while that of [^{111}In][In(pypa-C7-PSMA617)] was not determined due to unsuccessful separation of the transchelated ^{111}In and the radioactive complex with either PD10 column or iTLC-SA plate (EDTA and DTPA solution as mobile phase). The results are in significant contrast with the industrial "gold standard" macrocyclic chelator –DOTA – which required microwave heating at 80-100 ^{o}C over 20-30 minutes for quantitative radiolabeling with both ^{111}In and ^{177}Lu.[28, 40] DTPA and the cyclohexyl analogue (CHX-A"-DTPA) are two widely adopted non-macrocyclic ligands in ^{111}In radiopharmaceutical development in an effort to achieve high RCY at RT, but their inferior *in vitro* stabilities unfortunately limit their clinical potential (88.3% and 89.9% for [^{111}In][In(DTPA)]$^{2-}$ and [^{111}In][In(*p*-NH_2−Bn−CHX-A″−DTPA)]$^{2-}$, respectively, after 24 hours).[28, 29] Encouraging radiolabeling results with ^{111}In and ^{177}Lu were reported with H_4octapa, an octadentate ligand previously reported by our group with reported *in vitro* stability 92.3% and 87.7%, respectively, after one day.[2, 28] The nonadentate *p*-NO_2−Bn−neunpa was developed for ^{111}In with more favorable stability in human serum (97.8% over 5 days), but exhibited very low affinity to ^{177}Lu and therefore, further study was precluded.[29] As mentioned above, the apparent molar activity is a crucial parameter in preparing radiotracers. For [^{A}E][E(pypa-C7-PSMA617)] (^{A}E=^{177}Lu, ^{111}In), at the optimal radiolabeling concentration (i.e. 10^{-6} M), radiolabeling yields with different L/M ratios were tested using a mixture of no-carrier-added ^{177}Lu or ^{111}In, as well as non-radioactive ^{nat}Lu or ^{nat}In in an attempt to achieve the lowest L/M ratio. For both radiotracers, L/M ratio 2 has proved sufficient for ~98% RCY (RT), while equimolar gave only 76% ($^{111/nat}$In) and 72% RCY ($^{177/nat}$Lu). The results proved a cost-effective and comparable estimation for optimal radiometal-to-chelator ratio without consuming a large amount of radioactivity which is very expensive, while the resulting high apparent molar activity also conveniently obviates post-labeling purification, and thus further enhances their potential in the practical applications.

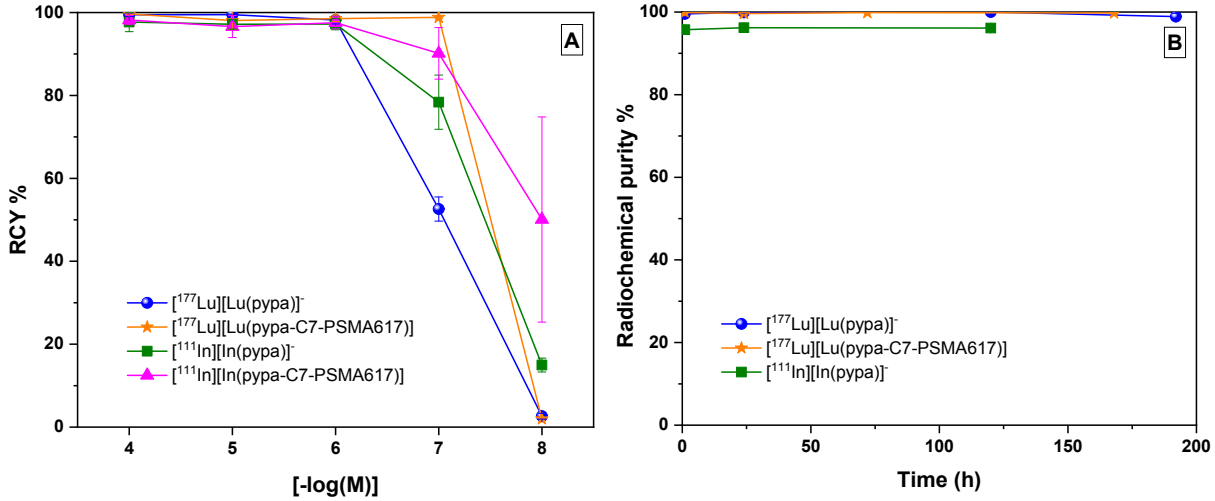

Figure 4. (A) Concentration dependent radiolabeling of H_4pypa and H_4pypa-C7-PSMA617 (10 minutes, room temperature) in NH_4OAc solution (0.15 M, pH = 7) with $^{177}Lu/^{111}In$. **(B)** Human serum challenge of the radiolabeled complexes over 5-7 days (37 °C).

SPECT/CT Imaging, Biodistribution Studies and Binding Affinity

[^{A}E(pypa-C7-PSMA617)] (^{A}E = ^{nat}In and ^{nat}Lu) inhibited the binding of ^{18}F-DCFPyL to PSMA on LNCaP cells in a dose-dependent manner (Figures S56-S57), and their calculated K_i values were 6.41 (1.80) nM and 7.88 (4.34) nM, respectively. For animal studies, ^{177}Lu- and ^{111}In-labeled radiotracers with apparent molar activities of 207 GBq/μmol and 459 GBq/μmol, respectively, were prepared and then injected into LNCaP-tumor-bearing mice (n=5 per time point). SPECT/CT imaging (Figure 5) and *ex vivo* biodistribution studies (Figure 6 and Table S6-S7) showed that both radioactive analogues excreted mainly via the renal pathway. The blood clearances for both radiotracers were fast, measured at 0.89±0.42% injected dose per gram (ID/g) at 4-hour post-injection (p.i.) and 1.04±0.34% ID/g at 1-hour p.i. for the ^{177}Lu- and ^{111}In-based tracers, respectively. In both cases, uptake in non-specific organs and tissues were low (e.g. fat, intestine, stomach, liver, pancreas, heart, muscle, bone), while high accumulations were observed in PSMA-expressing tissues (e.g. kidney, spleen, adrenal glands, LNCaP tumor).[41] For [^{177}Lu][Lu(pypa-C7-PSMA617)], the uptake in kidney, spleen, adrenal glands and tumors were 120±19% ID/g, 4.71±1.68% ID/g, 3.64±1.49% ID/g, 20.6±5.9% ID/g at 1-hour p.i., respectively. Except for tumor, in which the accumulation grew to 24.0±7.6% ID/g at 4-hour p.i. and then gradually reduced to 12.7±4.2% ID/g after 3 days, the uptake in other organs was rapidly cleared within the first 4 hours, resulting in a substantial increase in the tumor-to-background contrast ratio (Table S6). Moreover,

the tumor uptake was more than 60% higher than that of ^{177}Lu-PSMA-617 at both 4-hour and 72-hour p.i., which was reported with 14.5±1.8% ID/g and 7.80 ±3.69% ID/g, respectively.[42] Regarding [^{111}In][In(pypa-C7-PSMA617)], similar to its ^{177}Lu-counterpart, the background organs and tissues uptakes were low and cleared rapidly except in the kidney and tumor. After 24 hours, the kidney accumulation was 36.4±18.8% ID/g and the tumor uptake was 8.88±1.92% ID/g, leading to a tumor-to-kidney ratio of 0.24±0.10 compared to 6.70±1.75 for the ^{177}Lu-analogue (24-hour post-injection) (Tables S6-S7). A DOTA-based construct containing the same PSMA-targeting motif (Glu-urea-Lys) and IRDye800CW was synthesized and radiolabeled with ^{111}In as a dual-modality imaging agent.[43] The PC3-PIP tumor uptake was 14.6±1.3% ID/g at 24-hour p.i. and the calculated tumor-to-kidney ratio was around 0.3.[43] Schottelius et al. published a DOTA-based PSMA I&T which was metalated with ^{111}In, ^{177}Lu and ^{68}Ga.[44] In their case, [^{111}In]PSMA-I&T had the highest tumor uptake (~8% ID/g) at 1-hour p.i., along with the most kidney (~190% ID/g) and spleen (~46% ID/g) accumulation which was claimed to be CB17 SCID-mice related.[44]

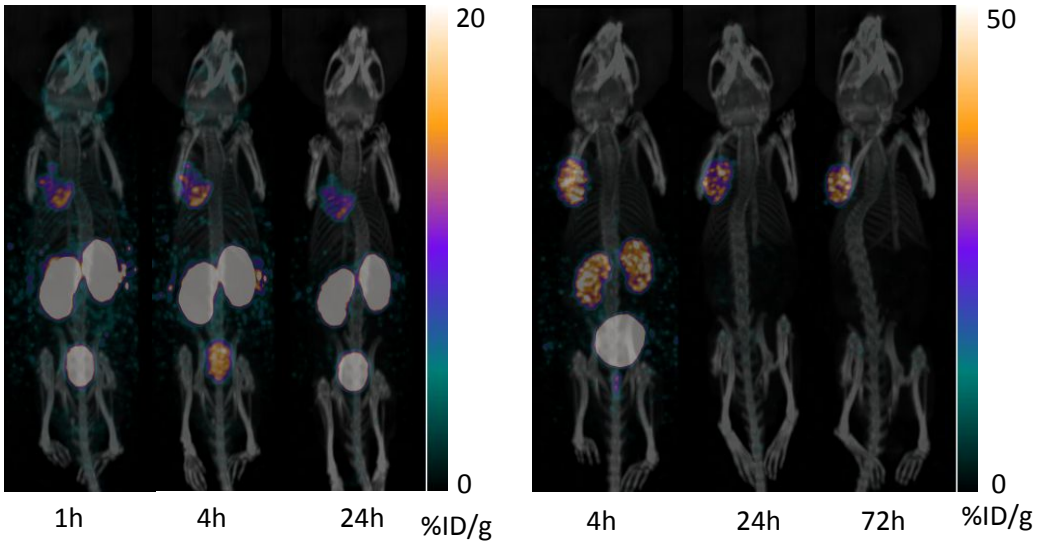

Figure 5. Representative SPECT/CT images (MIP, coronal) of [^{A}E][E(pypa-C7-PSMA617)] [^{A}E=^{111}In (left, 24.9 MBq), ^{177}Lu (right, 44.1 MBq)] in LNCaP-tumor-bearing mice at different p.i. time points.

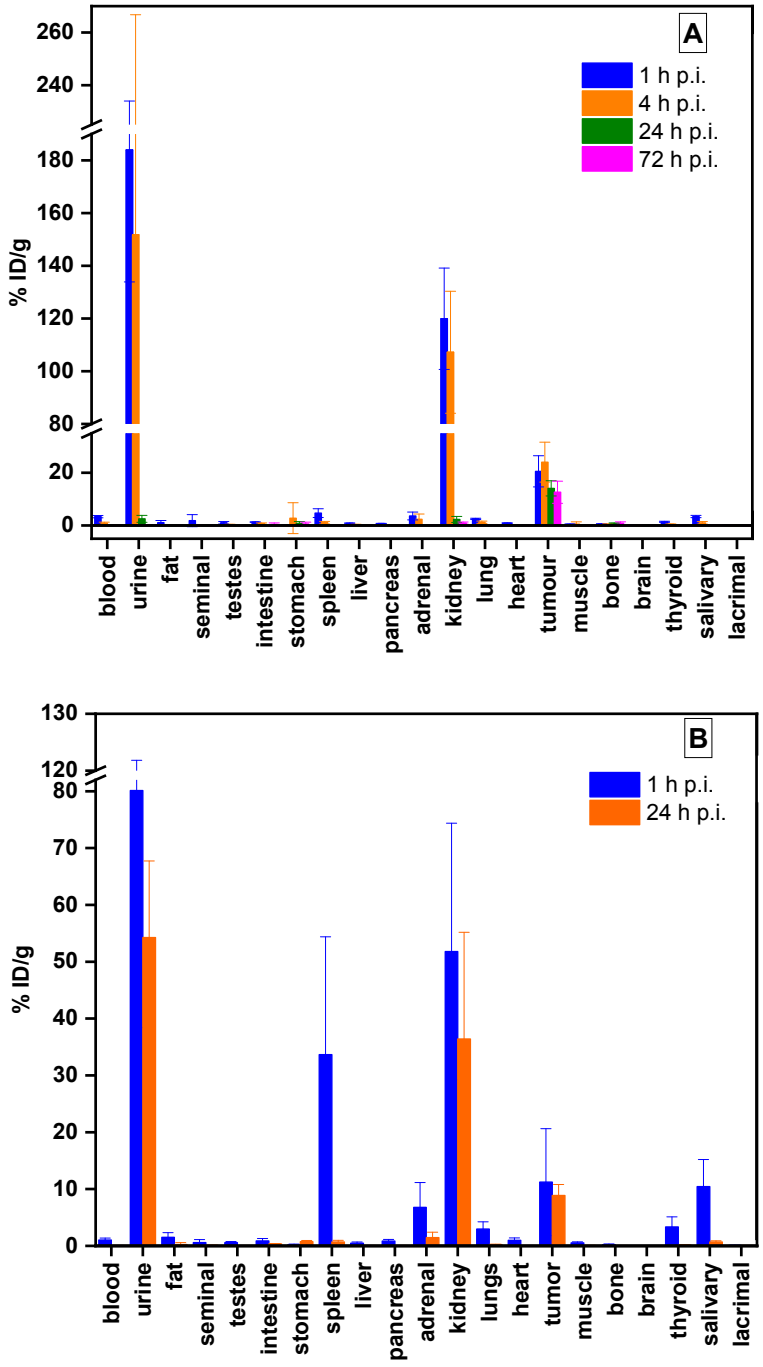

Figure 6. *Ex vivo* biodistribution data [^{A}E][E(pypa-C7-PSMA617)] [^{A}E=^{177}Lu **(A)**, ^{111}In **(B)**] in LNCaP-tumor-bearing mice at selected p.i. time points (n=5 per time point).

Conclusion

H_4pypa is a potentially nonadentate non-macrocyclic chelator with great affinity for ^{111}In and ^{177}Lu which are excellent radionuclides in cancer diagnosis and therapy. In addition to the quantitative

radiolabeling yields at fast complexation kinetics (10 minutes) under mild conditions (RT, pH = 7) with ^{111}In and ^{177}Lu, the corresponding H_4pypa complexes are highly thermodynamically stable and kinetically inert (<1% transmetalation to serum protein over 5-7 days), a benefit of the extra rigidity exerted by the central pyridyl moiety that serves as a cap to further stabilize the whole complex, as shown in the crystal structure of H[Lu(pypa)] where Lu is fully nine-coordinated by H_4pypa. Furthermore, the pM values of M^{3+}-H_4pypa systems ($M=In^{3+}$ (30.5), Lu^{3+} (22.6) and La^{3+} (19.9)) are much higher than those with DOTA, DTPA, H_4octapa, H_4octox and H_4neunpa. Moreover, inclusion of a *p*-OH group on the central pyridyl ring also renders H_4pypa a functionally versatile chelator. One of the main advantages is that the precursor (compound **14**) can be synthesized in large scale with excellent stability while any linker of interest can be attached easily, even in milligram scale, for fast screening. Here, an alkyl linker was selected to join the PSMA-targeting pharmacophore and the [^{A}E][E(pypa)] ($^{A}E=^{177}$Lu, ^{111}In) complexes demonstrating vastly different, but promising pharmacokinetics. In particular, the ^{177}Lu-counterpart shows significantly faster background clearance and higher tumor retention paving the way for potential theranostic applications. Beyond the proof-of-principle PSMA targeting, H_4pypa is also highly valuable for other types of cancer treatments, particularly radioimmunotherapy, in which a mild radiolabeling-condition is essential due to the temperature- and pH-sensitive antibody. Current efforts are expanding the applications of H_4pypa with other theranostic radionuclides (e.g. $^{44/47}$Sc, $^{86/90}$Y) and ^{225}Ac. Different bifunctional derivatives have been developed and conjugated to other targeting vectors, particularly to antibodies.

Experimental Section

Materials and Methods

All solvents and reagents were purchased from commercial suppliers (TCI America, Alfa Aesar, AK Scientific, Sigma-Aldrich, Fisher Scientific, Fluka) and were used as received. Human serum was purchased frozen from Sigma-Aldrich. The analytical thin-layer chromatography (TLC) plates used were aluminum-backed ultrapure silica gel 60 Å, 250 μm thickness; the flash column silica gel (standard grade, 60 Å, 32−63 mm) was provided by Silicycle. ^{1}H and ^{13}C NMR spectra were recorded at ambient temperature on Bruker AV300 and AV400 instruments, unless otherwise specified; the NMR spectra are expressed on the δ scale and were referenced to residual solvent peaks. Low-resolution (LR) mass spectrometry was performed using a Waters ZG spectrometer

with an ESCI electrospray/chemical-ionization source, and high-resolution electrospray ionization mass spectrometry (HR-ESI-MS) was performed on a Micromass LCT time-of-flight instrument at the Department of Chemistry, University of British Columbia. Microanalyses for C, H, and N were performed on a Carlo Erba Elemental Analyzer EA 1108. The HPLC system used for analysis and purification of non-radioactive compounds consisted of a Waters 600 controller, Waters 2487 dual wavelength absorbance detector, and a Waters delta 600 pump. Phenomenex Synergi 4 μ hydro-RP 80 Å column (250 mm × 21.2 mm semipreparative) was used for purification of deprotected H_4pypa and Phenomenex Luna 5 μm C18 100 Å LC column (250 mm × 10 mm) was used for purification of deprotected H_4pypa-C7-PSMA617. Automated column chromatography was performed using a Teledyne Isco (Lincoln, NE) Combiflash Rf automated system with solid load cartridges packed with Celite and RediSep Rf gold reusable normal-phase silica columns (Teledyne Isco, Lincoln, NE). Analyses of radiolabeled compounds were performed with both Instant TLC (iTLC) plates, impregnated with silic acid (iTLC-SA) purchased from Agilent Technologies and radio-HPLC. The TLC scanner model was BIOSCAN (system 200 imaging scanner) and the HPLC system was from Agilent Technologies (1200 series). Phenomenex Synergi 4 μ hydro-RP 80 Å column (250 mm × 4.60 mm) was used for separation of free radioactivity and radio-complex. $^{111}InCl_3$ was cyclotron-produced and provided by BWX Technologies as a ~0.05 M HCl solution; $^{177}LuCl_3$ was purchased from Isotope Technologies Garching (ITG). All the isotopes used were no-carrier added (n.c.a.). Deionized water was filtered through the PURELAB Ultra Mk2 system.

Di-tert-butyl pyridine-2,6-dicarboxylate (1). To a stirred suspension of 2,6-pyridinedicarboxylic acid (10.0 g, 59.8 mmol, 1 equiv.) in dichloromethane (DCM) (30 mL) was added tert-butyl alcohol (22.6 ml) and 4-dimethylaminopyridine (DMAP) (3.65 g, 29.9 mmol, 0.5 equiv.) at room temperature. Then, N,N'-dicyclohexylcarbodiimide (DCC) (27.2 g, 0.132 mol, 2.2 equiv.) in DCM (30 mL) was added dropwise using a dropping funnel over 1 hour. The mixture was left stirring at room temperature overnight, and then the precipitate was filtered off by vacuum filtration. The filtrate was concentrated *in vacuo* and then purified through a silica column (*CombiFlash* R_f automated column system, 80 g gold silica column, DCM - methanol (MeOH), 0-5% MeOH). The product fractions were rotary-evaporated to give an off-white solid (8.36 g, 50%). ^{1}H NMR (400 MHz, 298 K, $CDCl_3$): δ 8.18 (d, J = 7.8 Hz, 2H), 7.95 – 7.90 (m, 1H), 1.64 (s, 18H). ^{13}C NMR (75

MHz, 298 K, $CDCl_3$): δ 168.3, 150.0, 138.1, 127.3, 83.2, 27.9. LR-ESI-MS: calcd for $[C_{15}H_{21}NO_4 + H]^+$ 280.1; found $[M + H]^+$ 280.2

Tert-butyl 6-(hydroxymethyl)picolinate (2). Compound **1** (1.40 g, 5.00 mmol, 1 equiv.) was dissolved in dry MeOH (150 mL) in a round-bottom flask. $NaBH_4$ (0.189 g, 5.00 mmol, 1 equiv.) was added at 0 °C. The mixture was stirred at room temperature for 1 hour and then another equiv. of $NaBH_4$ was added. The reduction continued until the mono-reduced picolinate dominated, as monitored by silica TLC (5% MeOH in DCM). The average reaction time was 3-4 hours. After that, the reaction mixture was diluted with DCM (100 mL) and then quenched with saturated $NaHCO_3$ in water (100 mL). The organic phase was separated and the bulk of MeOH in the aqueous phase was removed *in vacuo* to give an aqueous layer which was then extracted with DCM (100 mL × 3). The combined organic phases were dried over anhydrous Na_2SO_4, and then clarified by filtration. The filtrate was concentrated and then purified through a silica column (*CombiFlash* R_f automated column system, 40 g gold silica column, DCM : MeOH, 0-5 % MeOH). The product fractions were rotary evaporated to give an off-white powder (2.25 g, 72 %).^{1}H NMR (400 MHz, 298 K, $CDCl_3$): δ 7.88 (d, J = 7.6 Hz, 2H), 7.77 (t, J = 7.7 Hz, 1H), 7.46 (d, J = 7.7 Hz, 1H), 4.82 (s, 2H), 1.59 (s, 9H). ^{13}C NMR (75 MHz, 298 K, $CDCl_3$): δ 164.1, 160.3, 148.3, 137.6, 123.6, 123.4, 82.4, 64.5, 28.2. LR-ESI-MS : calcd for $[C_{11}H_{15}NO_3 + Na]^+$ 232.1; found $[M + Na]^+$ 232.2

Tert-butyl 6-formylpicolinate (3). To a round-bottom flask with a stirred solution of compound **2** (4.50 g, 21.5 mmol, 1 equiv.) in 1,4-dioxane (50 mL) was added SeO_2 (1.19 g, 10.8 mmol, 0.5 equiv.). The mixture was refluxed at 100 °C overnight. After the reaction completed, the hot mixture was clarified by filtering through a Celite bed and the filtrate was concentrated *in vacuo*. The crude mixture was purified through a silica column (*CombiFlash* R_f automated column system, 80 g gold silica column, hexanes : ethyl acetate (Hex : EtOAc), 0-60 % EtOAc) to give a pale yellow solid (2.51 g, 56 %). ^{1}H NMR (400 MHz, 298 K, $CDCl_3$): δ 10.19 (s, 1H), 8.25 (d, J = 6.6 Hz, 1H), 8.11 (d, J = 8.8 Hz, 1H), 8.01 (t, J = 7.7 Hz, 1H), 1.67 (s, 9H). ^{13}C NMR (75 MHz, 298 K, $CDCl_3$): δ 193.2, 163.3, 152.9, 150.1, 138.3, 128.7, 123.9, 83.2, 28.2. LR-ESI-MS : calcd for $[C_{11}H_{13}NO_3 - H]^+$ 206.1; found $[M - H]^+$ 206.1

Tert-butyl 6-(((2-(tert-butoxy)-2-oxoethyl)amino)methyl)picolinate (4). To a round-bottom flask with a stirred solution of compound **3** (0.500 g, 2.40 mmol, 1 equiv.) in dry MeOH (20 mL)

was added tert-butyl glycinate (0.320 g, 2.40 mmol, 1 equiv.). The mixture was stirred for one hour at room temperature and then sodium cyanoborohydride ($NaBH_3CN$) (0.31 g, 4.87 mmol, 2 equiv.) was added. The reduction reaction was continued for three hours at room temperature before quenching with saturated $NaHCO_3$ in water (10 mL) and then extraction with DCM (20 mL × 3). The combined organic phases were dried over anhydrous Na_2SO_4, and then clarified by filtration. The filtrate was concentrated *in vacuo* and the residue was purified through a silica column (*CombiFlash* R_f automated column system, 12 g gold silica column, DCM : MeOH, 0-5% MeOH). The product fractions were combined and rotary-evaporated to give a pale yellow oil (0.55 g, 70%).^{1}H NMR (400 MHz, 298 K, $CDCl_3$): δ 7.76 (d, J = 7.7 Hz, 1H), 7.65 (t, J = 7.7 Hz, 1H), 7.43 (d, J = 7.6 Hz, 1H), 3.91 (s, 2H), 3.26 (s, 2H), 1.48 (s, 9H), 1.32 (s, 9H).^{13}C NMR (75 MHz, 298 K, $CDCl_3$): δ 171.1, 163.9, 159.7, 148.6, 137.2, 124.9, 123.0, 81.9, 81.0, 54.2, 51.0, 27.9. LR-ESI-MS: calcd for $[C_{17}H_{26}N_2O_4 + H]^+$ 323.2; found $[M + H]^+$ 323.1

2,6-Di(hydroxymethyl)pyridine (5). To a round-bottom flask with a stirred mixture of pyridine-2,6-dicarboxylic acid dimethyl ester (3.00 g, 15.4 mmol, 1 equiv.) in dry MeOH (50 mL) at 0 °C was slowly added $NaBH_4$ (2.33 g, 61.5 mmol, 4 equiv.) in three portions over 15 minutes. The solution was then stirred at room temperature for 12 hours. $CHCl_3$ (25 mL) was added followed by saturated Na_2CO_3 in water (50 mL) to quench the reaction. The organic phase was separated and the MeOH in the aqueous phase was removed *in vacuo* to give a concentrated aqueous solution which was then extracted with $CHCl_3$ (100 mL × 10). Multiple extractions were required to recover most of the product. The combined organic phases were dried over anhydrous Na_2SO_4, and then clarified by filtration. The filtrate was concentrated to give a white solid (1.99 g, 92%). ^{1}H NMR (400 MHz, 298 K, $CDCl_3$): δ 7.70 (t, J = 7.7 Hz, 1H), 7.20 (d, J = 7.7 Hz, 2H), 4.79 (s, 4H). ^{13}C NMR (75 MHz, 298 K, MeOD) δ 161.5, 139.2, 120.2, 65.5. LR-ESI-MS: calcd for $[C_7H_9NO_2 + H]^+$ 140.1; found $[M + H]^+$ 140.1

2,6-Bis(bromomethyl)pyridine (6). To a three-neck round-bottom flask with a stirred solution of compound **5** (3.00 g, 21.2 mmol, 1 equiv.) in dry ACN (acetonitrile)/$CHCl_3$ (30 mL, 50:50 v/v) at 0 °C was added PBr_3 (6.02 mL, 63.4 mmol, 3 equiv.) dropwise using a dropping funnel over 15 minutes. The mixture was refluxed for 18 hours, and then cooled before water (20 mL) was added slowly at 0 °C to quench the reaction. After extraction with $CHCl_3$ (50 mL × 3), the combined organic layers were dried over anhydrous $MgSO_4$, and then clarified by filtration. The solvent was

removed under reduced pressure and the product was obtained as a pure white solid (4.88 g, 87%). ^{1}H NMR (400 MHz, 298 K, $CDCl_3$): δ 7.76 (t, J = 7.8 Hz, 1H), 7.43 (d, J = 7.8 Hz, 2H), 4.59 (s, 4H). ^{13}C NMR (75 MHz, 298 K, $CDCl_3$) δ 156.8, 138.5, 123.1, 33.3. LR-ESI-MS: calcd for $[C_7H_7Br_2N + H]^+$ 263.9; found $[M(^{79}Br) + H]^+$ 263.9

Di-tert-butyl-6,6'-(((pyridine-2,6-diylbis(methylene))-bis((2-(tert-butoxy)-2-oxoethyl)aza-nedi-yl))bis(methylene))dipicolinate (7). To a round-bottom flask with a stirred solution of compound **6** (1.00 g, 3.80 mmol, 1 equiv) in dry ACN (15 mL) was added K_2CO_3 (1.38 g, 11.4 mmol, 3 equiv.), followed by compound **4** (2.45 g, 7.60 mmol, 2 equiv.) and KI (1.26 g, 7.60 mmol, 2 equiv.). The mixture was stirred at 40 °C for 24 hours, and then K_2CO_3 was separated by centrifugation, followed by washing with DCM/ACN (10 mL × 3). The organic phase was concentrated *in vacuo* and then purified through a silica column (*CombiFlash* R_f automated column system, 24 g gold silica column, DCM : MeOH, 0-8% MeOH). The product fractions were rotary-evaporated to give a yellow oil (1.99 g, 70%). ^{1}H NMR (400 MHz, 298 K, $CDCl_3$): δ 7.93 – 7.76 (m, 4H), 7.61 (t, J = 7.6 Hz, 1H), 7.49 (d, J = 7.4 Hz, 2H), 7.12 (d, J = 7.7 Hz, 2H), 4.23 (s, 4H), 3.97 (s, 4H), 3.18 (s, 4H), 1.32 (s, 18H), 1.24 (s, 18H). ^{13}C NMR (75 MHz, 298 K, $CDCl_3$): δ 169.8, 164.7, 157.3, 157.0, 145.9, 138.1, 137.3, 126., 122.9, 121.8, 80.7, 58.5, 58.1, 53.6, 53.1, 51.9. LR-ESI-MS: calcd for $[C_{41}H_{57}N_5O_8 + Na]^+$ 770.4; found $[M + Na]^+$ 770.4

H_4pypa (8). Compound **7** (37.6 mg, 5.03 × 10^{-5} mol) was dissolved in DCM (1 mL) in a round-bottom flask and TFA (1 mL) was added dropwise to the stirred solution using a Pasteur pipette. The mixture was stirred overnight at room temperature and then rotary-evaporated. The residue was redissolved in H_2O (2 mL) and then purified through reverse phase HPLC (A: ACN, B: H_2O/0.1% TFA, 5-50% A over 30 minutes, 10 mL/minute, t_R = 16.8 minutes) (18.4 mg, 70%). ^{1}H NMR (400 MHz, 298 K, D_2O): δ 8.16 – 8.03 (m, 4H), 7.92 (t, J = 7.8 Hz, 1H), 7.74 (d, J = 7.0 Hz, 2H), 7.49 (d, J = 7.9 Hz, 2H), 4.78 (s, 4H), 4.71 (s, 4H), 4.19 (s, 4H). ^{13}C NMR (75 MHz, 298 K, D_2O): δ 169.8, 166.3, 150.3, 150.2, 146.3, 141.2, 140.9, 128.2, 125.5, 125.0, 58.1, 58.0, 55.2. HR-ESI-MS: calcd for $[C_{25}H_{25}N_5O_8 + H]^+$ 524.1781; found $[M + H]^+$ 524.1783. Elemental analysis: calcd % for H_4pypa·2TFA·1.7H_2O ($C_{29}H_{30.4}F_6N_5O_{13.7}$ = 782.1739): C 44.53, H 3.92, N 8.95; found: C 44.86, H 3.59, N 8.63.

Na[^{nat}In(pypa)] Compound **8** (9.60 mg, 1.26 × 10^{-5} mol, 1 equiv.) was dissolved in H_2O (0.5 mL) in a scintillation vial and 0.1 M NaOH (aq) was added to adjust the pH to 7. $In(NO_3)_3 \cdot 6H_2O$ (6.17

mg, 1.51 × 10^{-5} mol, 1.2 equiv.) was added. The mixture was stirred at room temperature for 1 hour and the complexation was confirmed by LR-ESI-MS. ^{1}H NMR (400 MHz, 298 K, D_2O): δ 8.26 (t, *J* = 7.7 Hz, 1H), 8.20 – 8.15 (m, 2H), 8.02 – 7.94 (m, 2H), 7.88-7.83 (m, 2H), 7.50 (d, *J* = 7.7 Hz, 1H), 7.34 (d, *J* = 7.9 Hz, 1H), 4.44 (d, *J* = 17.4 Hz, 1H), 4.10 (d, *J* = 17.4 Hz, 1H), 3.91 (d, *J* = 17.1 Hz, 1H), 3.78 (d, *J* = 17.1 Hz, 1H), 3.22 (d, *J* = 17.5 Hz, 1H), 2.94 (d, *J* = 17.7 Hz, 1H). ^{13}C NMR (100 MHz, 298 K, D_2O): δ 176.7, 176.2, 168.3, 168.2, 154.0, 153.9, 153.2, 152.9, 145.1, 144.9, 142.5, 142.4, 142.2, 128.0, 127.7, 124.99, 123.48, 123.0, 117.8, 61.0, 60.7, 59.6, 57.4, 57.3, 54.8. HR-ESI-MS: calcd for $[C_{25}H_{21}{}^{115}InN_5O_8 + 2Na]^+$ 680.0224; found $[M + 2Na]^+$ 680.0223.

Na[^{nat}Lu(pypa)] Compound **8** (13.6 mg, 1.79 × 10^{-5} mol, 1 equiv.) was dissolved in H_2O (0.5 mL) in a scintillation vial and 0.1 M NaOH (aq) was added to adjust the pH to 7. $Lu(NO_3)_3 \cdot 6H_2O$ (9.23 mg, 1.97 x 10^{-5} mol, 1.1 equiv.) was added. The mixture was stirred at room temperature for 1 hour and the complexation was confirmed by LR-ESI-MS. ^{1}H NMR (400 MHz, 298 K, D_2O): δ 8.21 (t, *J* = 7.8 Hz, 2H), 8.05 (d, *J* = 7.6 Hz, 2H), 7.85 (t, *J* = 7.8 Hz, 1H), 7.80 (d, *J* = 7.8 Hz, 2H), 7.44 (d, *J* = 7.8 Hz, 2H), 4.66 (d, *J* = 2.6 Hz, 4H), 4.39 (d, *J* = 14.7 Hz, 2H), 4.07 (d, ^{2}J = 14.7 Hz, 2H), 3.98 (d, ^{2}J = 16.6 Hz, 2H), 3.49 (d, ^{2}J = 17.0 Hz, 2H). ^{13}C NMR (100 MHz, 298 K, D_2O): δ 179.1, 173.1, 156.5, 152.7, 150.5, 141.6, 140.0, 125.5, 124.0, 123.0, 64.6, 64.5, 63.4. HR-ESI-MS: calcd for $[C_{25}H_{21}{}^{175}LuN_5O_8 + 2H]^+$ 696.0954; found $[M + 2H]^+$ 696.0956.

Na[^{nat}La(pypa)] Compound **8** (13.5 mg, 1.79 × 10^{-5} mol, 1 equiv.) was dissolved in H_2O (0.5 mL) in a scintillation vial and 0.1 M NaOH (aq) was added to adjust the pH to 6. $La(ClO_4)_3 \cdot 6H_2O$ (10.7 mg, 1.97 x 10^{-5} mol, 1.1 equiv.) was added. The mixture was stirred at room temperature for 1 hour and the complexation was confirmed by LR-ESI-MS. ^{1}H NMR (400 MHz, 298 K, D_2O): δ 8.07 (t, *J* = 7.7 Hz, 1H), 7.98 (d, *J* = 8.4 Hz, 1H), 7.80 (s, 2H), 7.75 (t, *J* = 7.7 Hz, 1H), 7.67 (d, *J* = 7.8 Hz, 1H), 7.44 (d, *J* = 7.7 Hz, 1H), 7.26 (d, *J* = 8.3 Hz, 1H), 7.17 (s, 1H), 4.62 (d, *J* = 16.2 Hz, 1H), 4.50 (d, *J* = 14.0 Hz, 1H), 4.22 (d, *J* = 16.0 Hz, 1H), 4.06 (d, *J* = 18.6 Hz, 2H), 3.85 (d, *J* = 14.1 Hz, 4H), 3.64 (d, *J* = 16.3 Hz, 1H), 3.09 (s, 2H). ^{13}C NMR (100 MHz, 298 K, D_2O): δ 180.2, 173.4, 156.6, 156.1, 150.0, 145.3, 140.4, 126.5, 125.0, 123.7, 123.6, 123.3, 123.2, 63.5, 63.4, 62.5, 62.2. HR-ESI-MS: calcd for $[C_{25}H_{21}{}^{139}La\ N_5O_8 + 2Na]^+$ 704.0249; found $[M + 2Na]^+$ = 704.0251.

Dimethyl 4-hydroxypyridine-2,6-dicarboxylate (9). Thionyl chloride ($SOCl_2$) (9.50 mL, 0.130 mol, 5 equiv.) was added slowly using a syringe to a stirred suspension of chelidamic acid monohydrate (5.28 g, 26.2 mmol, 1 equiv.) in MeOH (60 mL) in a two-neck round-bottom flask at 0 °C. The mixture was stirred at room temperature for 24 hours and then refluxed for an additional 2 hours. The solvent was removed under reduced pressure gently at room temperature and then D.I. water was added at 0 °C. The mixture was neutralized with 1 M K_2CO_3 in water solution and the precipitate was filtered by vacuum filtration, and then washed with 50% MeOH in water solution (~10 mL). The white precipitate was dried under reduced pressure to give a white solid (5.54 g, >99 %). ^{1}H NMR (400 MHz, 298 K, $(CD_3)_2SO$): δ 6.74 (s, 2H), 3.72 (s, 6H). ^{13}C NMR (75 MHz, 298 K, $(CD_3)_2SO$): δ 165.7, 149.2, 116.6, 52.7. LR-ESI-MS : calcd for $[C_9H_9NO_5 + Na]^+$ 234.0; found $[M + Na]^+$ 234.2

Dimethyl 4-(benzyloxy)pyridine-2,6-dicarboxylate (10). To a round-bottom flask with a stirred solution of compound **9** (1.65 g, 7.82 mmol, 1 equiv.) in dry ACN was added anhydrous K_2CO_3 (2.19 g, 15.8 mmol, 2.02 equiv.) and benzyl bromide (1.02 mL, 8.60 mmol, 1.1 equiv.). The reaction mixture was refluxed overnight at 60 °C. K_2CO_3 was filtered out by vacuum filtration and then washed with DCM. The filtrate was concentrated *in vacuo* and then purified through a silica column (*CombiFlash* R_f automated column system, 24 g gold silica column, DCM : MeOH, 0-5 % MeOH). The product fractions were rotary-evaporated to give a white powder (1.51 g, 64 %). ^{1}H NMR (400 MHz, 298 K, $CDCl_3$): δ 7.90 (s, 2H), 7.44-7.38 (m, 5H), 5.23 (s, 2H), 4.01 (s, 6H). ^{13}C NMR (75 MHz, 298 K, $CDCl_3$): δ 150.0, 129.0, 128.9, 127.9, 115.0, 71.0, 53.4. LR-ESI-MS : calcd for $[C_{16}H_{15}NO_5 + Na]^+$ 324.1; found $[M + Na]^+$ 324.1

(4-(Benzyloxy)pyridine-2,6-diyl)dimethanol (11). To a round-bottom flask with a stirred solution of compound **10** (8.74 g, 29.0 mmol, 1 equiv.) in dry MeOH (90 mL) was added $NaBH_4$ (3.29 g, 87.1 mmol, 3 equiv.) in three portions over 30 minutes at 0 °C. The reaction mixture was stirred at room temperature. After 24 hours, the mixture was diluted with $CHCl_3$ (50 mL) and then quenched with saturated aqueous $NaHCO_3$ (50 mL). The organic phase was separated and the bulk of MeOH in the aqueous layer was removed *in vacuo* to give an aqueous solution which was extracted with $CHCl_3$ (50 mL × 4). The combined organic phases were dried over anhydrous Na_2CO_3, and then clarified by filtration. The filtrate was rotary-evaporated to give a white solid (5.86 g, 82 %).^{1}H NMR (400 MHz, 298 K, $CDCl_3$): δ 7.42-7.35 (m, 5H), 6.79 (s, 2H), 5.12 (s,

2H), 4.70 (s, 4H). ^{13}C NMR (75 MHz, 298 K, $CDCl_3$): δ 184.4, 166.5, 162.7, 160.6, 149.6, 135.6, 128.9, 128.6, 127.6, 117.2, 111.8, 107.7, 106.5, 106.1, 105.2, 70.2, 64.5. LR-ESI-MS: calcd for $[C_{14}H_{15}NO_3 + Na]^+$ 268.1; found $[M + Na]^+$ 268.2

4-(Benzyloxy)-2,6-bis(bromomethyl)pyridine (12). Compound **11** (1.76 g, 12.6 mmol, 1 equiv.) was suspended in dry ACN/dry $CHCl_3$ (40 mL, 50:50 v/v) in a three-neck round-bottom flask. PBr_3 (3.60 mL, 37.9 mmol, 3 equiv.) in $CHCl_3$ (5 mL) was added dropwise using a dropping funnel to the stirred solution of compound **11** at 0 °C over 15 minutes. The reaction mixture was stirred at 60 °C for 18 hours and then saturated aqueous Na_2CO_3 was added slowly to quench the reaction at 0 °C. The aqueous phase was extracted with $CHCl_3$ (50 mL × 3). The combined organic phases were dried over anhydrous Na_2SO_4, and then clarified by filtration. The filtrate was rotary-evaporated to yield a colorless oil which later solidified to a white solid (3.28 g, 70 %). ^{1}H NMR (400 MHz, 298 K, $CDCl_3$): δ 7.43 (m, 5H), 7.36 (s, 2H), 5.37 (s, 2H), 4.95 (s, 4H). ^{13}C NMR (75 MHz, 298 K, $CDCl_3$): δ 170.9, 154.5, 133.2, 129.5, 129.3, 128.3, 113.2, 73.0, 25.3. LR-ESI-MS: calcd for $[C_{14}H_{13}{}^{79}Br_2NO + H]^+$ 369.9; found $[M(^{79}Br) + H]^+$ 369.9

Di-tert-butyl-6,6'-((((4-(benzyloxy)pyridine-2,6-diyl)bis(methylene))bis((2-(tert-butoxy)-2-oxoethyl)azanediyl))bis(methylene))dipicolinate (13). Compound **12** (0.400 g, 1.30 mmol, 1 equiv.), K_2CO_3 (595 mg, 4.31 mmol, 3.3 equiv.) and KI (434 mg, 2.61 mmol, 2 equiv.) were added sequentially to the stirred solution of compound **4** (0.837 g, 2.60 mmol, 2 equiv.) in dry ACN (15 mL) in a round-bottom flask. The mixture was stirred at 30 °C for 24 hours. K_2CO_3 was removed by centrifugation and then washed with DCM/ACN (10 mL × 3). The combined supernatants were concentrated *in vacuo* and then purified with a silica column (*CombiFlash* R_f automated column system, 12 g gold silica column, DCM : MeOH, 0-5% MeOH). The product fractions were rotary-evaporated to give a pale yellow oil (0.67 g, 73 %). ^{1}H NMR (400 MHz, 298 K, $CDCl_3$): δ 7.92-7.61 (m, 6H), 7.52-7.30 (m, 5H), 7.12 (s, 2H), 5.11 (s, 2H), 4.03 (s, 4H), 3.86 (s, 4H), 3.33 (s, 4H), 1.57 (s, 18H), 1.43 (s, 18H). ^{13}C NMR (75 MHz, 298 K, $CDCl_3$): δ 170.5, 166.2, 164.0, 160.2, 148.6, 137.2, 136.1, 128.5, 128.1, 127.7, 125.6, 123.3, 123.0, 107.8, 81.8, 80.9, 69.7, 64.4, 59.8, 56.1, 53.4, 28.0. LR-ESI-MS: calcd for $[C_{48}H_{63}N_5O_9 + Na]^+$ 876.5; found $[M + Na]^+$ 876.6

Di-tert-butyl-6,6'-((((4-hydroxypyridine-2,6-diyl)bis(methylene))bis((2-(tert-butoxy)-2-oxoethyl)azanediyl))bis(methylene))dipicolinate (14). Compound **13** (0.170 g, 0.200 mmol) was dissolved in dry MeOH (20 mL) in a three-neck round-bottom flask, saturated with N_2(g). Pd/C

(10 % w/w, 0.1 equiv.) was added under a stream of N_2(g). The flask was purged with N_2(g), followed by H_2(g) from a balloon. The mixture was stirred vigorously at room temperature overnight under H_2 atmosphere, and then Pd/C was filtered off through a Celite bed, washed with MeOH (10 mL × 5). The filtrate was rotary-evaporated to a pale-yellow oil (0.150 g) and used without purification. LR-ESI-MS: calcd for $[C_{41}H_{57}N_5O_9 + H]^+$ 764.4; found $[M + H]^+$ 764.6

Benzyl 8-bromooctanoate (15). 8-Bromooctanoic acid (2.00 g, 8.96 mmol, 1 equiv.), benzyl alcohol (0.930 ml, 8.96 mmol, 1 equiv.) and a catalytic amount of DMAP (0.1-0.2 equiv.) were dissolved sequentially in dry DCM (20 mL) in a round-bottom flask. DCC (2.04 g, 9.86 mmol, 1.1 equiv.) in DCM (10 mL) was added dropwise using a dropping funnel over 1 hour. The mixture was stirred at room temperature for 24 hours. The white precipitate was filtered off by filtration and then the solvent was evaporated *in vacuo*. The residue was purified with a silica column (*CombiFlash* R_f automated column system, 24 g gold silica column, DCM : MeOH, 0 - 5 % MeOH). The product fractions were rotary-evaporated to yield a colorless oil (2.51 g, 89 %). ^{1}H NMR (400 MHz, 298 K, $CDCl_3$): δ 7.35-7.32 (m, 5H), 5.12 (s, 2H), 3.39 (t, J = 6.8 Hz, 2H), 2.36 (t, J = 7.5 Hz, 2H), 1.83 (p, J = 6.9 Hz, 2H), 1.69 – 1.61 (m, 2H), 1.44-1.40 (m, 2H), 1.32 (dt, J = 7.3, 3.5 Hz, 4H). ^{13}C NMR (75 MHz, 298 K, $CDCl_3$): δ 173.7, 136.2, 128.7, 128.3, 66.3, 34.4, 34.0, 32.8, 29.0, 28.5, 28.1, 24.9. LR-ESI-MS: calcd for $[C_{15}H_{21}BrO_2 + Na]^+$ 335.1; found $[M + Na]^+$ 335.1

Di-tert-butyl-6,6'-((((4-((8-(benzyloxy)-8-oxooctyl)oxy)pyridine-2,6-diyl)bis-(methylene))bis-((2-(tert-butoxy)-2-oxoethyl)azanediyl))-bis(methylene))-di-picolinate (16). To a round-bottom flask with a stirred solution of compound **14** (152 mg, 0.200 mmol, 1 equiv.) in dry tetrahydrofuran (THF) (4 mL) was added anhydrous K_2CO_3 (82.6 mg, 0.600 mmol, 3 equiv.). The mixture was stirred for 1 hour before the addition of compound **15** (65.6 mg, 0.210 mmol, 1.05 equiv.). The mixture was stirred for 24 hours at 30 ºC, followed by separation of K_2CO_3 by centrifugation. The isolated salt was washed with DCM twice (~5 mL each) while the combined organic phases were concentrated *in vacuo* to a yellow oil. The product crude was characterized by MS and NMR, and then used directly in the next step (0.195 g, 90%). ^{1}H NMR (400 MHz, 298 K, $CDCl_3$): δ 7.85 – 7.80 (m, 4H), 7.72 (t, J = 7.7 Hz, 2H), 7.34-7.27 (m, 5H), 6.98 (s, 2H), 5.09 (s, 2H), 4.02 (s, 4H), 3.96 (t, J = 6.4 Hz, 2H), 3.84 (s, 4H), 3.32 (s, 4H), 2.34 (t, J = 7.5 Hz, 2H), 1.77 – 1.70 (m, 2H), 1.66-1.58 (m, 24H), 1.42 (s, 18H), 1.34 – 1.32 (m, 4H). ^{13}C NMR (75

MHz, 298 K, $CDCl_3$): δ 173.6, 170.6, 166.7, 164.2, 160.4, 160.2, 148.7, 137.3, 136.1, 128.6, 128.2, 125.7, 123.1, 107.7, 82.0, 81.0, 67.9, 66.1, 64.3, 59.9, 56.2, 34.3, 29.1, 28.1, 25.9, 25.4, 24.9. LR-ESI-MS: calcd for $[C_{56}H_{77}N_5O_{11} + H]^+$ 996.6; found $[M + H]^+$ 996.7

8-((2,6-Bis(((2-(tert-butoxy)-2-oxoethyl)((6-(tert-butoxycarbonyl)pyridin-2-yl)methyl)-amino)methyl)pyridin-4-yl)oxy)octanoic acid (17). Compound **16** (94.8 mg, 0.0952 mmol) was dissolved in dry MeOH (7 mL) in a three-neck round-bottom flask, saturated with N_2(g). Pd/C (10 % w/w) was added under a stream of N_2. The flask was purged with N_2(g) again, followed by H_2(g) from a balloon. The mixture was stirred vigorously at room temperature overnight under H_2 atmosphere, and then Pd/C was filtered off through a Celite bed, washed with MeOH(10 mL × 5). The filtrate was concentrated *in vacuo* to a pale-yellow oil (75.70 mg, 88 %) and used without purification. LR-ESI-MS: calcd for $[C_{49}H_{71}N_5O_{11} + Na]^+$ 928.5; found $[M + Na]^+$ 928.7

^{t}Bu$_4$pypa-C7-NHS (18). To a two-neck round-bottom flask with a stirred solution of compound **17** (75.7 mg, 0.0837 mmol, 1 equiv.) in dry ACN (2 mL) was added N-hydroxysuccinimide (10.6 mg, 0.0922 mmol, 1.1 equiv.) and EDCI (19.2 mg, 0.101 mmol, 1.2 equiv.) under N_2 (g). The mixture was stirred at room temperature under an inert atmosphere overnight. Then, the solvent was removed *in vacuo* and the residue was redissolved in DCM (10 mL), and then washed with water (10 mL × 3) and brine (10 mL × 2). The combined organic phases were dried over anhydrous Na_2SO_4, and then clarified by filtration. The filtrate was rotary-evaporated to yield a yellow oil (71.70 mg, 86 %) which was used in next step without further purification. ^{1}H NMR (400 MHz, 298 K, $CDCl_3$): δ 7.92 – 7.77 (m, 4H), 7.77 – 7.67 (m, 2H), 6.98 (s, 2H), 4.11 – 3.92 (m, 6H), 3.83 (s, 4H), 3.30 (s, 4H), 2.79 (s, 4H), 2.59 – 2.54 (m, 2H), 1.76 – 1.69 (m, 4H), 1.56 (s, 18H), 1.40 (s, 24H). ^{13}C NMR (75 MHz, 298 K, $CDCl_3$): δ 173.7, 170.7, 169.3, 168.7, 164.2, 160.4, 148.8, 137.4, 128.7, 128.3, 125.8, 123.2, 82.1, 81.1, 77.4, 66.2, 60.0, 56.4, 31.0, 29.8, 29.0, 28.8, 28.3, 28.2, 25.9, 25.7, 24.6. HR-ESI-MS: calcd $[C_{53}H_{75}N_6O_{13} + H]^+$ 1003.5392 found $[M + H]^+$ 1003.5358

Solid Phase Peptide Coupling. Solid-phase synthesis of H_4pypa-C7-PSMA617 was modified from literature procedures.[26] Fmoc-Lys(ivDde)-Wang resin (0.046 mmol, 0.61 mmol/g loading) was suspended in dimethylformamide (DMF) for 30 minutes. Fmoc was then removed by treating the resin with 20% piperidine in DMF (3 × 8 minutes). The isocyanate derivative of di-t-butyl ester of glutamate (0.138 mmol, 3 equiv.) was prepared according to literature procedures[26] and added to the lysine-immobilized resin to react for 16 hours. After washing the resin with DMF, the ivDde-

protecting group was removed with 2% hydrazine in DMF (5 × 5 minutes), followed by coupling of Fmoc-2-Nal-OH and Fmoc-tranexamic acid to the side chain of Lys using Fmoc-protected amino acid (0.138 mmol, 3 equiv.), N,N,N',N'-tetramethyl-O-(1H-benzotriazol-1-yl)uronium hexafluorophosphate (HBTU) (0.138 mmol, 3 equiv.), hydroxybenzotriazole (HOBt) (0.138 mmol, 3 equiv.) and N,N-diisopropylethylamine (DIPEA) (0.368 mmol, 8 equiv.). Afterwards, the chelator $^{t}Bu_4$pypa-C7-NHS (0.138 g, 0.138 mmol) was coupled to the peptide-bound resin by using DIPEA (0.460 mmol, 10 equiv.) in DMF overnight. The peptide was then deprotected and simultaneously cleaved from the resin by treating with 95/5 TFA/triisopropylsilane (TIS) for 2 hours at room temperature. After filtration, the peptide was precipitated by adding cold diethyl ether to the TFA solution. The crude peptide was purified by semi-preparative HPLC (32% acetonitrile in water containing 0.1% TFA at a flow rate of 4.5 mL/minute, t_R = 8.8 minutes). The eluates containing the desired peptide were collected, pooled, and lyophilized (5.16 mg, 3.91 μmol, 8.5%) HR-ESI-MS: calcd $[C_{66}H_{82}N_{10}O_{19} + H]^+$ 1319.5836; found $[M+H]^+$ 1319.7376.

X-ray Crystallography. Single orange colored rhombic-shaped crystals of **H[Lu(pypa)]** were obtained by the slow evaporation of 1:1 $LuCl_3$ and H_4pypa solutions in water after adjustment of pH to 2. A suitable crystal 0.15×0.05×0.01 mm^3 was selected and mounted on a suitable support on a Bruker APEX-II CCD diffractometer. The crystal was kept at a steady T = 90(2) K during data collection. The structure was solved with the **ShelXT**[45]structure solution program using the dual solution method and by using **Olex2**[46] as the graphical interface. The model was refined with version 2018/1 of **ShelXL**[45] using Least Squares minimisation.

Solution Thermodynamics. All potentiometric titrations were carried out with a Metrohm Titrando 809 and a Metrohm Dosino 800 with a Ross combined electrode. A 20 mL and 25 ºC thermostated glass cell with an inlet-outlet tube for nitrogen gas (purified through a 10% NaOH solution to exclude any CO_2 prior to and during the course of the titration) was used as a titration cell. The electrode was calibrated daily in hydrogen ion concentration by direct titration of HCl with freshly prepared NaOH solution and the results were analyzed with Gran procedure[47] in order to obtain the standard potential Eº and the ionic product of water pK_w at 25 °C and 0.16 M NaCl as a supporting electrolyte. Solutions were titrated with carbonate-free NaOH (0.16 M) that was standardized against freshly recrystallized potassium hydrogen phthalate. The experimental

procedures for determination of the ligand protonation constants, complex formation constants and pM values are described in the supporting information.

Radiolabeling and Human Serum Challenge Experiments. Generally, for concentration-dependent radiolabeling, an aliquot of a ligand solution (25 μL) of desired concentration was mixed with ^{177}Lu/^{111}In (~2 MBq) and diluted to a final volume (250 μL) with ammonium acetate solution (0.15 M, pH=7). The final mixture was incubated at room temperature for 10 minutes before determination of radiochemical yield with iTLC-SA plate and radio-HPLC (Detailed procedures of concentration- and ratio-dependent radiolabeling are described in the Supporting Information). For the human serum challenge, to a quantitative radiolabeled complex solution was added an equal volume of human serum. The mixture was incubated at 37 ^{o}C and an aliquot of the mixture was spotted on iTLC-SA plate at desired time-point to determine the amount of intact complex (%) (A detailed procedure is described in the Supporting Information).

SPECT/CT Imaging, Biodistribution Studies and Binding Affinity. Imaging and biodistribution experiments were performed using NODSCID IL2RγKO male mice. The mice were maintained, and the experiments were conducted according to the guidelines established by the Canadian Council on Animal Care and approved by Animal Ethics Committee of the University of British Columbia (A detailed procedure is described in the Supporting Information). SPECT/CT imaging experiments were conducted using the MILabs (Utrecht, The Netherlands) U-SPECT+/CT scanner. Each tumor bearing mouse was injected with ^{111}Lu/^{111}In labeled H_4pypa-C7-PSMA617 (44.1 MBq for ^{177}Lu and 24.9 MBq for ^{111}In) through the tail vein under anesthesia of 2% isoflurane in oxygen. The mice were allowed to recover and roam freely in their cage and imaged at 1, 4, 24, and 72 hours after injection. At each time point, the mice were sedated again with 2% isoflurane in oxygen and positioned in the micro scanner (A detailed procedure is described in the Supporting Information). For *in vitro* competition binding assays, non-specific binding was determined in the presence of non-radiolabeled DCFPyL (10 μM). The assay mixtures were further incubated for 1 hour at 37 °C with gentle agitation. Then, the buffer and hot ligand were removed, and cells were washed twice with cold HEPES buffered saline. Trypsin solution (400 μl, 0.25%) was then added to each well to harvest the cells. Radioactivity was measured on the gamma counter. Data analyses of K_i were performed using the nonlinear regression algorithm of GraphPad Prism 7 software (A detailed procedure is described in the Supporting Information).

Acknowledgements

We thank the team of animal technicians and veterinarians for helpful assistance at the BC Cancer Research Center and Dr. Maria Ezhova for her useful advice on NMR experiments at UBC. We gratefully acknowledge funding from NSERC CREATE IsoSiM at TRIUMF for PhD research stipends (LL, NC), MITACS for Globalink student support (NC), both NSERC and CIHR for financial support via a Collaborative Health Research Project (CHRP to FB, CO and PS) and NSERC Discovery (CO).

Author Information Notes

*Corresponding Authors : fbenard@bccrc.ca, orvig@chem.ubc.ca

ORCID

Lily Li : 0000-0002-8779-8689

Maria de Guadalupe Jaraquemada-Peláez : 0000-0002-6204-707X

Neha Choudhary : 0000-0003-2838-6606

Chris Orvig : 0000-0002-2830-5493

Notes: The authors declare no competing financial interest.

Associated Content (52 pages)

Supporting Information

Representative spectra of the in batch acidic titration of H_4pypa; titration curve of an acidic solution of H_4pypa; speciation plots of H_4pypa calculated with protonation constants on Table 2; representative spectra of the in batch UV-titration of the M^{3+}-pypa (M=In, Lu, La) systems as the pH is raised; protonation constants and stability constants of ttha^{6-} ligand and its complexes with In^{3+} and Lu^{3+} metal ions; stepwise protonation constants (log K_{HqL}) of ligands and the corresponding complexes with La^{3+}, Lu^{3+} and In^{3+}. NMR spectra (^{1}H, ^{13}C{^{1}H}, HSQC, COSY) of compounds **1-18** and the [M(pypa)]$^-$ (M=In, Lu, La) complexes; high resolution mass spectra of compounds **8, 18** and H_4pypa-C7-PSMA617, as well as the [M(pypa)]$^-$ (M=In, Lu, La) complexes; radiochemical-yield data and radio-HPLC spectra of [^{A}E][E(pypa)]$^-$ and [^{A}E][E(pypa-C7-PSMA617)]$^-$ (^{A}E=^{111}In, ^{177}Lu) complexes; biodistribution studies data (%ID/g) of [^{A}E][E(pypa-

C7-PSMA617)]$^{-}$ (^{A}E=^{111}In, ^{177}Lu) complexes and binding affinity graphs of [M(pypa-C7-PSMA617)]$^{-}$ (M=^{nat}In, ^{nat}Lu); crystallographic data of H[Lu(pypa)]. Experimental procedures of solutions studies of [M(pypa)]$^{-}$ (M=In, Lu, La) complexes, radiolabeling studies and *in vitro* human serum challenge of [^{A}E][E(pypa)]$^{-}$ and [^{A}E][E(pypa-C7-PSMA617)]$^{-}$ (^{A}E=^{111}In, ^{177}Lu) complexes, *in vitro* competition binding assays of [M(pypa-C7-PSMA617)]$^{-}$ (M=In, Lu) complexes, radiotracers, [^{A}E][E(pypa-C7-PSMA617)]$^{-}$ (^{A}E=^{111}In, ^{177}Lu), preparation for biodistribution studies, biodistribution studies and SPECT/CT imaging studies.

References :

1. Yeong, C.-H., Cheng, M.-h., and Ng, K.-H. (2014) Therapeutic radionuclides in nuclear medicine: current and future prospects. *J. Zhejiang. Univ-Sc B. 15*, 845-863.

2. Price, E. W., Zeglis, B. M., Cawthray, J. F., Ramogida, C. F., Ramos, N., Lewis, J. S., Adam, M. J., and Orvig, C. (2013) H_4octapa-Trastuzumab: Versatile Acyclic Chelate System for ^{111}In and ^{177}Lu Imaging and Therapy. *J. Am. Chem. Soc. 135*, 12707-12721.

3. Price, E. W., and Orvig, C. (2014) Matching chelators to radiometals for radiopharmaceuticals. *Chem. Soc. Rev. 43*, 260-290.

4. Ramogida, C. F., and Orvig, C. (2013) Tumour targeting with radiometals for diagnosis and therapy. *Chem Commun. 49*, 4720-4739.

5. Xu, L.-C., Ritter, A., and Chelius, E. (2015) An Improved Kit Formulation for the Preparation of ^{99m}Tc-EC0652. *J. Nucl. Med. 56*, 1165-1165.

6. Schottelius, M., Schwaiger, M., and Wester, H.-J., (2003) Rapid and high-yield solution-phase synthesis of DOTA-Tyr3-octreotide and DOTA-Tyr3-octreotate using unprotected DOTA. *Tetrahedron Lett. 44*, 2393-2396.

7. Vallabhajosula, S., Nikolopoulou, A., Jhanwar, Y. S., Kaur, G., Tagawa, S. T., Nanus, D. M., Bander, N. H., Goldsmith, S. J. (2016) Radioimmunotherapy of Metastatic Prostate Cancer with ^{177}Lu-DOTAhuJ591 Anti Prostate Specific Membrane Antigen Specific Monoclonal Antibody. *Curr. Radiopharm. 9*, 44-53.

8. Guleria, M., Das, T., Kumar, C., Amirdhanayagam, J., Sarma, H. D., and Banerjee, S. (2017) Preparation of clinical-scale ^{177}Lu-Rituximab: Optimization of protocols for conjugation, radiolabeling, and freeze-dried kit formulation. *J. Label. Compd. Radiopharm. 60*, 234-241.

9. De Jong, M., Breeman, W. A. P., Valkema, R., Bernard, B. F., and Krenning, E. P. (2005) Combination Radionuclide Therapy Using ^{177}Lu- and ^{90}Y-Labeled Somatostatin Analogs. *J. Nucl.Med. 46*, 13S-17S.

10. Liu, F., Zhu, H., Yu, J., Han, X., Xie, Q., Liu, T., Xia, C., Li, N., and Yang, Z. (2017) ^{68}Ga/^{177}Lu-labeled DOTA-TATE shows similar imaging and biodistribution in neuroendocrine tumor model. *Tumor Biol. 39*, 1010428317705519.

11. Banerjee, S., Pillai, M. R. A., and Knapp, F. F. (2015) Lutetium-177 Therapeutic Radiopharmaceuticals: Linking Chemistry, Radiochemistry, and Practical Applications. *Chem. Rev. 115*, 2934-2974.

12. Kostelnik, T. I., and Orvig, C. (2019) Radioactive Main Group and Rare Earth Metals for Imaging and Therapy. *Chem Rev. 119*, 902-956.

13. Hashimoto, K., Matsuoka, H., and Uchida, S. (2003) Production of no-carrier-added ^{177}Lu via the ^{176}Yb(n, γ)^{177}Yb & → ^{177}Lu process. *J. Radioanal. Nucl. Chem. 255*, 575-579.

14. Piroozfar, B., Raisali, G., Alirezapour, B., and Mirzaii, M. (2018) The effect of ^{111}In radionuclide distance and auger electron energy on direct induction of DNA double-strand breaks: a Monte Carlo study using Geant4 toolkit. *Int. J. Radiat. Biol. 94*, 385-393.

15. Cornelissen, B., Waller, A., Target, C., Kersemans, V., Smart, S., and Vallis, K. A. (2012) (111)In-BnDTPA-F3: an Auger electron-emitting radiotherapeutic agent that targets nucleolin. *EJNMMI Res. 2*, 9-9.

16. McLean, J. R., Blakey, D. H., Douglas, G. R., and Bayley, J. (1989) The Auger Electron Dosimetry of Indium-111 in Mammalian Cells in Vitro. *Radiat Res. 119*, 205-218.

17. Cardinal Health. (2018) FDA-approved radiopharmaceuticals (https://www.cardinalhealth.com/content/dam/corp/web/documents/fact-sheet/cardinal-health-fda-approved-radiopharmaceuticals.pdf, accessed on 23/02/2019)

18. Siegel, R. L., Miller, K. D., and Jemal, A. (2017) Cancer statistics, 2017. *CA. Cancer. J. Clin. 67*, 7-30.

19. Silver, D. A., Pellicer, I., Fair, W. R., Heston, W. D., and Cordon-Cardo, C. (1997) Prostate-specific membrane antigen expression in normal and malignant human tissues. *Clin. Cancer Res. 3*, 81.

20. Han, M., and Partin, A. W. (2001) Current Clinical Applications of the In-capromab Pendetide Scan (ProstaScint(R) Scan, Cyt-356). *Rev Urol. 3*, 165-171.

21. Hillier, S. M., Maresca, K. P., Femia, F. J., Marquis, J. C., Foss, C. A., Nguyen, N., Zimmerman, C. N., Barrett, J. A., Eckelman, W. C., and Pomper, M. G. et al. (2009) Preclinical Evaluation of Novel Glutamate-Urea-Lysine Analogues That Target Prostate-Specific Membrane Antigen as Molecular Imaging Pharmaceuticals for Prostate Cancer. *Cancer Res. 69*, 6932.

22. Maresca, K. P., Hillier, S. M., Femia, F. J., Keith, D., Barone, C., Joyal, J. L., Zimmerman, C. N., Kozikowski, A. P., Barrett, J. A., and Eckelman, W. C. et al. (2009) A Series of Halogenated Heterodimeric Inhibitors of Prostate Specific Membrane Antigen (PSMA) as Radiolabeled Probes for Targeting Prostate Cancer. *J. Med. Chem. 52*, 347-357.

23. Benešová, M., Schäfer, M., Bauder-Wüst, U., Afshar-Oromieh, A., Kratochwil, C., Mier, W., Haberkorn, U., Kopka, K., and Eder, M. (2015) Preclinical Evaluation of a Tailor-Made DOTA-Conjugated PSMA Inhibitor with Optimized Linker Moiety for Imaging and Endoradiotherapy of Prostate Cancer. *J. Nucl. Med. 56*, 914-920.

24. Baranski, A.-C., Schäfer, M., Bauder-Wüst, U., Wacker, A., Schmidt, J., Liolios, C., Mier, W., Haberkorn, U., Eisenhut, M., and Kopka, K. et al. (2017) Improving the Imaging Contrast of ^{68}Ga-PSMA-11 by Targeted Linker Design: Charged Spacer Moieties Enhance the Pharmacokinetic Properties. *Bioconjugate Chem. 28*, 2485-2492.

25. Kuo, H.-T., Pan, J., Zhang, Z., Lau, J., Merkens, H., Zhang, C., Colpo, N., Lin, K.-S., and Benard, F. (2018) Effects of linker modification on tumor-to-kidney contrast of ^{68}Ga-labeled PSMA-targeted imaging probes. *Mol Pharm. 15*, 3502-3511.

26. Benešová, M., Bauder-Wüst, U., Schäfer, M., Klika, K. D., Mier, W., Haberkorn, U., Kopka, K., and Eder, M. (2016) Linker Modification Strategies To Control the Prostate-Specific Membrane Antigen (PSMA)-Targeting and Pharmacokinetic Properties of DOTA-Conjugated PSMA Inhibitors. *J. Med. Chem. 59*, 1761-1775.

27. Umbricht, C. A., Benešová, M., Schibli, R., and Müller, C. (2018) Preclinical Development of Novel PSMA-Targeting Radioligands: Modulation of Albumin-Binding Properties To Improve Prostate Cancer Therapy. *Mol. Pharm. 15*, 2297-2306.

28. Price, E. W., Cawthray, J. F., Bailey, G. A., Ferreira, C. L., Boros, E., Adam, M. J., and Orvig, C. (2012) H_4octapa: An Acyclic Chelator for ^{111}In Radiopharmaceuticals. *J. Am. Chem. Soc. 134*, 8670-8683.

29. Spreckelmeyer, S., Ramogida, C. F., Rousseau, J., Arane, K., Bratanovic, I., Colpo, N., Jermilova, U., Dias, G. M., Dude, I., Jaraquemada-Peláez, M. d. G. et al. (2017) *p*-NO_2–Bn–H_4neunpa and H_4neunpa–Trastuzumab: Bifunctional Chelator for Radiometalpharmaceuticals and ^{111}In Immuno-Single Photon Emission Computed Tomography Imaging. *Bioconjuate Chem. 28*, 2145-2159.

30. Wang, X., Jaraquemada-Peláez, M. d. G., Cao, Y., Pan, J., Lin, K.-S., Patrick, B. O., and Orvig, C. (2019) H_2hox: Dual-Channel Oxine-Derived Acyclic Chelating Ligand for ^{68}Ga Radiopharmaceuticals. *Inorg Chem. 58*, 2275-2285.

31. Shannon, R. D. (1976) Revised effective ionic radii and systematic studies of interatomic distances in halides and chalcogenides. *Acta Crystallogr A. 32*, 751-767.

32. Gans, P., Sabatini, A., and Vacca, A. (1999) Determination of equilibrium constants from spectrophometric data obtained from solutions of known pH: The program pHab. *Ann. Chim-Rome*. 89, 45-49.

33. Gans, P., Sabatini, A., and Vacca, A. (1996) Investigation of equilibria in solution. Determination of equilibrium constants with the HYPERQUAD suite of programs. *Talanta. 43*, 1739-1753.

34. Alderighi, L., Gans, P., Ienco, A., Peters, D., Sabatini, A., and Vacca, A. (1999) Hyperquad simulation and speciation (HySS): a utility program for the investigation of equilibria involving soluble and partially soluble species. *Coord. Chem. Rev. 184*, 311-318.

35. Jaraquemada-Peláez, M. d. G., Wang, X., Clough, T. J., Cao, Y., Choudhary, N., Emler, K., Patrick, B. O., and Orvig, C. (2017) H_4octapa: synthesis, solution equilibria and complexes with useful radiopharmaceutical metal ions. *Dalton Trans. 46*, 14647-14658.

36. Harris, W. R., Carrano, C. J., and Raymond, K. N. (1979) Spectrophotometric determination of the proton-dependent stability constant of ferric enterobactin. *J. Am. Chem. Soc. 101*, 2213-2214.

37. Wang, X., Jaraquemada-Peláez, M. d. G., Rodríguez-Rodríguez, C., Cao, Y., Buchwalder, C., Choudhary, N., Jermilova, U., Ramogida, C. F., Saatchi, K., and Häfeli, U. O. et al. (2018) H_4octox: Versatile Bimodal Octadentate Acyclic Chelating Ligand for Medicinal Inorganic Chemistry. *J. Am. Chem. Soc. 140*, 15487-15500.

38. Chakraborty, S., Chakravarty, R., Shetty, P., Vimalnath, K. V., Sen, I. B., and Dash, A., (2016) Prospects of medium specific activity ^{177}Lu in targeted therapy of prostate cancer using ^{177}Lu-labeled PSMA inhibitor. *J. Label. Compd. Radiopharm. 59*, 364-371.

39. Fendler, W. P., Stuparu, A. D., Evans-Axelsson, S., Lückerath, K., Wei, L., Kim, W., Poddar, S., Said, J., Radu, C. G., and Eiber, M. et al. (2017) Establishing ^{177}Lu-PSMA-617 Radioligand Therapy in a Syngeneic Model of Murine Prostate Cancer. *J. Nucl. Med. 58*, 1786-1792.

40. Breeman, W. A. P., de Jong, M., Visser, T. J., Erion, J. L., and Krenning, E. P. (2003) Optimising conditions for radiolabelling of DOTA-peptides with ^{90}Y, ^{111}In and ^{177}Lu at high specific activities. *Eur. J. Nucl. Med. Mol. Imaging. 30*, 917-920.

41. Harada, N., Kimura, H., Onoe, S., Watanabe, H., Matsuoka, D., Arimitsu, K., Ono, M., and Saji, H. (2016) Synthesis and Biologic Evaluation of Novel ^{18}F-Labeled Probes Targeting Prostate-Specific Membrane Antigen for PET of Prostate Cancer. *J. Nucl. Med. 57*, 1978-1984.

42. Kuo, H.-T., Merkens, H., Zhang, Z., Uribe, C. F., Lau, J., Zhang, C., Colpo, N., Lin, K.-S., and Bénard, F. (2018) Enhancing Treatment Efficacy of ^{177}Lu-PSMA-617 with the Conjugation of an Albumin-Binding Motif: Preclinical Dosimetry and Endoradiotherapy Studies. *Mol Pharm. 15*, 5183-5191.

43. Banerjee, S. R., Pullambhatla, M., Byun, Y., Nimmagadda, S., Foss, C. A., Green, G., Fox, J. J., Lupold, S. E., Mease, R. C., and Pomper, M. G. (2011) Sequential SPECT and Optical Imaging of Experimental Models of Prostate Cancer with a Dual Modality Inhibitor of the Prostate-Specific Membrane Antigen. *Angew. Chem. Int. Edit. 50*, 9167-9170.

44. Schottelius, M., Wirtz, M., Eiber, M., Maurer, T., and Wester, H.-J. (2015) [^{111}In]PSMA-I&T: expanding the spectrum of PSMA-I&T applications towards SPECT and radioguided surgery. *EJNMMI Res. 5*, 68.

45. G. M. Sheldrick. (2015) SHELXT - Integrated space-group and crystal-structure determination. *Acta Cryst. A71*, 3-8

46. Dolomanov, O. V., Bourhis, L. J., Gildea, R. J., Howarda, J. A. K., and Puschmanna, H. (2009) OLEX2: a complete structure solution, refinement and analysis program. *J. Appl. Crystallogr. 42*, 339-341

47. Gran, G. (1952) Determination of the equivalence point in potentiometric titrations. Part II. *Analyst. 77*, 661-671

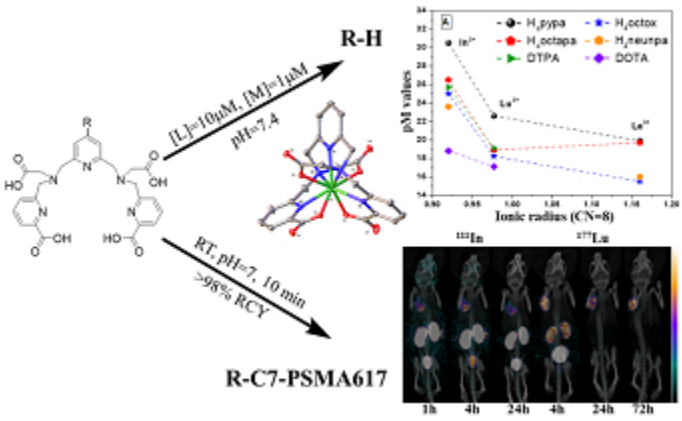

TOC graphic

71x43mm (120 x 120 DPI)